Available online at www.sciencedirect.com

ScienceDirect

Geochimica et Cosmochimica Acta 148 (2015) 159–178

Geochimica et Cosmochimica Acta

www.elsevier.com/locate/gca

The paradox between low shock-stage and evidence for compaction in CM carbonaceous chondrites explained by multiple low-intensity impacts

Paula Lindgren [a,*], Romy D. Hanna [b], Katherine J. Dobson [c,d], Tim Tomkinson [e], Martin R. Lee [a]

[a] School of Geographical and Earth Sciences, University of Glasgow, Glasgow G12 8QQ, UK
[b] Jackson School of Geological Sciences, University of Texas, Austin, TX 78712, USA
[c] Manchester X-ray Imaging Facility, School of Materials, University of Manchester, Manchester M13 9PL, UK
[d] Research Complex at Harwell, Rutherford Appleton Laboratories, Oxfordshire OX11 0FA, UK
[e] Scottish Universities Environmental Research Centre, East Kilbride E75 0QF, UK

Received 9 March 2014; accepted in revised form 7 September 2014; available online 18 September 2014

Abstract

Petrographic analysis of eight CM carbonaceous chondrites (EET 96029, LAP 031166, LON 94101, MET 01072, Murchison, Murray, SCO 06043, QUE 93005) by electron imaging and diffraction, and X-ray computed tomography, reveals that six of them have a petrofabric defined by shock flattened chondrules. With the exception of Murchison, those CMs that have a strong petrofabric also contain open or mineralized fractures, indicating that tensional stresses accompanying the impacts were sufficient to locally exceed the yield strength of the meteorite matrix. The CMs studied span a wide range of petrologic subtypes, and in common with Rubin (2012) we find that the strength of their petrofabrics increases with their degree of aqueous alteration. This correspondence suggests that impacts were responsible for enhancing alteration, probably because the fracture networks they formed tapped fluid reservoirs elsewhere in the parent body. Two meteorites that do not fit this pattern are MET 01072 and Murchison; both have a strong petrofabric but are relatively unaltered. In the case of MET 01072, impact deformation is likely to have postdated parent body aqueous activity. The same may also be true for Murchison, but as this meteorite also lacks fractures and veins, its chondrules were most likely flattened by multiple low intensity impacts. Multiphase deformation of Murchison is also revealed by the microstructures of calcite grains, and chondrule-defined petrofabrics as revealed by X-ray computed tomography. The contradiction between the commonplace evidence for impact-deformation of CMs and their low shock stages (most belong to S1) can be explained by most if not all having been exposed to multiple low intensity (i.e., <5 GPa) shock events. Aqueous alteration was enhanced by those impacts that were of sufficient intensity to open high permeability fracture networks that could connect to fluid reservoirs.

1. INTRODUCTION

1.1. Impacts and parent body evolution

Impacts have been important in the evolution of asteroids throughout solar system history. For example, they have been responsible for the transfer of material between

* Corresponding author. Tel.: +44 1413305442.
E-mail address: paula.lindgren@glasgow.ac.uk (P. Lindgren).

http://dx.doi.org/10.1016/j.gca.2014.09.014
0016-7037/

bodies, as witnessed by meteorite breccias that contain clasts of other meteorite types, e.g., Kaidun (Zolensky et al., 1991; Zolensky and Ivanov, 2003) and the howardites (Reid et al., 1990; Brearley and Papike, 1993). With regards to individual bodies, impacts have comminuted and mixed material within their regoliths (i.e., regolith 'gardening'), and have led to compaction, fracturing, fragmentation, heating and possibly also aqueous alteration of their interiors (e.g., Kerridge and Bunch, 1979; Metzler et al., 1992).

The role of impacts in parent body evolution can also be explored by determining the magnitude of shock pressure that a meteorite has experienced. Shock pressures can be quantified by analysing the microstructures of plagioclase feldspar and olivine (where present). Changes to these minerals are used to define six shock stages, termed S1–S6, where S1 is unshocked (i.e., the silicate minerals have experienced <5 GPa) (Stöffler et al., 1991). Different meteorite groups have evidence for contrasting ranges of shock; for example ordinary chondrites are typically more highly shocked than carbonaceous chondrites, and within the carbonaceous chondrite group the CV3s are more highly shocked than the CO3s and CM2s (Scott et al., 1992). Of the 23 CM2 meteorites studied by Scott et al. (1992) only one had a shock stage greater than S1, which implies that hypervelocity impacts played a minor role in the evolution of the parent bodies of aqueously altered carbonaceous chondrites. However, compactional petrofabrics are commonplace in CM meteorites (Table 1), and have been attributed to either impact or lithostatic processes. The importance of distinguishing between these two agents of compaction has been recently highlighted by Rubin (2012), who suggested that impacts had generated the aqueous solutions that mediated alteration of the CMs (e.g., by melting of H_2O-rich ice and/or dehydration of phyllosilicates) and facilitated their movement within the parent body (i.e., by generating high permeability fracture networks). ALH 88045 is one example of a highly altered CM meteorite with flattened chondrules, but that shows no other evidence of shock deformation (Zolensky et al., 1997).

The aim of the present study is to reconcile this contradiction between the evidence for compaction of the CMs (i.e., presence of petrofabrics) and their low shock stage, and we test three possible explanations: (i) the petrofabrics formed by lithostatic compaction rather than by hypervelocity impacts (Table 1); (ii) the petrofabrics formed by low shock pressures, which themselves may be due to attenuation of a higher magnitude shock wave by the porous meteorite matrix (Rubin, 2012); (iii) the petrofabrics formed by multiple episodes of low intensity shock, rather than by a single higher intensity event. In order to evaluate these possibilities we have sought to understand better the degree and mechanism(s) of compaction of carbonaceous chondrite parent bodies by quantification of chondrule deformation and associated petrofabrics of eight CMs. We have focused our attention on chondrule deformation because Tomeoka et al. (1999) and Nakamura et al. (2000) showed experimentally that carbonaceous chondrite chondrules are flattened in the plane of the shock wave, and that their aspect ratios change in a regular manner as pressures increase. Thus, deformed chondrules may be used as a semi-quantitative measure of the magnitude and orientation of the shock wave(s).

1.2. The Murchison paradox

Murchison is one of the eight meteorites studied, and is particularly important for efforts to understand deformation of the CMs, owing to the controversy over the magnitude of shock pressure that it has experienced. It is one of the least aqueously altered CMs known (i.e., CM2.5; Rubin et al., 2007) and so according to the model of Rubin (2012) it should be unshocked; indeed he found that it lacks a petrofabric and most of its olivine grains belong to S1. Scott et al. (1992), however, classified Murchison as S1–S2 breccia, indicating that some regions or clasts had been shocked to >5 GPa. As only 10–20% of the chondrules they examined contained olivine grains with S2 microstructures, Scott et al. (1992) suggested that they had been shocked prior to incorporation into the Murchison parent body. They examined but rejected an alternative explanation that the chondrules had been shocked *in situ* but experienced different pressures owing to the heterogeneous nature of the passage of the shock wave through the parent body. The *ex situ* shock hypothesis of Scott et al. (1992) is supported by the findings of Roth et al. (2011) that ~20% of Murchison chondrules have pre-compaction exposure ages of up to 30 million years, whereas the others yield cosmogenic ages of ~1.5 million years. Thus, it may be that the highly shocked subset of Murchison chondrules also spent a long time in the regolith where they were exposed to more impacts and/or higher intensities of shock than the S1 chondrules. Taken together, the work of Scott et al. (1992) and Roth et al. (2011) suggests that conventional shock classifications may be inappropriate for quantifying the paleostress histories of meteorites such as the CMs that can have complex regolith histories.

Here we have asked if there is any evidence for *in situ* shock deformation of Murchison, and have used two novel and complementary techniques to document the magnitude, frequency and orientation of any compaction events: (i) determination of the aspect ratios and relative orientations (i.e., petrofabrics) of chondrules in 3D by high resolution X-ray computed tomography (XCT) – this work draws on the initial XCT findings by Hanna et al. (2012) of a foliation fabric in Murchison, and (ii) paleostress analysis using the *e*-twin microstructures of calcite as revealed by electron backscatter diffraction (EBSD). Calcite microstructures can provide an independent measure of the magnitude of shock deformation, and as the threshold pressure for twin formation is ~0.1 to 0.5 GPa (Lindgren et al., 2013b) they are sensitive to much lower pressures than olivine microstructures or chondrule flattening. Calcite can also provide information about the orientation of the shock wave from analysis of which of the three possible *e*-twin orientations that have been activated. Furthermore, since calcite is a product of aqueous processing, it will only record syn- or post-alteration shock (Lindgren et al., 2011).

Table 1
Petrographic indicators of compaction in CM meteorites.

Stress indicator(s)	Meteorite	Suggested origin of petrofabric
Flattened chondrules and CAIs	Cold Bokkeveld (CM2.2; S1)[a], ALH 83100 (CM2.1)[b]; EET 90047 (CM1/2) [b]; Y-793321 (CM2)[c]; MET 01072 (CM2.3)[d]	Lithostatic compaction[b]; Impact[c,d]
Flattened aggregates (including chondrule pseudomorphs and serpentine-tochilinite 'clumps')	ALH 88045 (CM2.0)[b]; EET 83334 (CM2.0)[b]; QUE 97990 (CM2.6)[e]; Y-71198 (CM2.4)[e]; SCO 06043 (CM2.0)[f]	Lithostatic compaction[b]; Impact[e]
Foliation defined by chondrules, chondrule fragments, chondrule pseudomorphs, refractory inclusions, amoeboid olivine inclusions, opaque grains and PCP clumps	MET 01070 (CM2.0)[g]; LAP 02277 (CM2.0)[g]; QUE 93005 (CM2.1)[g]; QUE 99355 (CM2.3)[g]; Cold Bokkeveld (CM2.2; S1)[g]; Murchison (CM2.5; S1-S2 breccia)[h]	Impact[g]
Crystallographic orientation of aragonite	Murray (CM2.4–2.5; S1)[i]	Lithostatic compaction[i]
Crystallographic orientation of serpentine	Murchison (CM2.5; S1-S2 breccia)[j]; Y-74642 (CM2)[k]	Lithostatic compaction[j,k]
Anisotropy of magnetic susceptibility (AMS)	Acfer 331 (CM2)[l]; DaG 557 (CM2)[l]	Impacts[l]
Deformed calcite vein	LON 94101 (CM2.3)[m,n]	Multiple phases of impact[m]

Where known, the petrologic subtype (after Rubin et al., 2007) and shock stage (after Scott et al., 1992), are indicated in parentheses. CM1/2 and CM2 denotes that the subtype has not been determined.
[a] Greenwood et al. (1994).
[b] Zolensky et al. (1997).
[c] Nakamura (2006).
[d] Nakamura et al. (2012).
[e] Trigo-Rodriguez et al. (2006).
[f] Lindgren et al. (2012).
[g] Rubin (2012).
[h] Hanna et al. (2012).
[i] Lee and Ellen (2008).
[j] Fujimura et al. (1983).
[k] Fujimura et al. (1982).
[l] Gattacceca et al. (2005).
[m] Lindgren et al. (2011).
[n] Lee et al. (2013).

2. MATERIALS AND METHODS

2.1. Sample preparation

This study used seven standard one inch round polished thin sections of CM carbonaceous chondrites. These samples were selected because they cover the entire spectrum of degrees of aqueous alteration according to the scheme of Rubin et al. (2007). Six are loans from the NASA Antarctic meteorite collection: Scott Glacier (SCO) 06043, 10 (weathering grade B/Ce); LaPaz Icefield (LAP) 031166, 15 (weathering grade B); Meteorite Hills (MET) 01072, 14 (weathering grade B); Queen Alexandra Range (QUE) 93005, 10 (weathering grade A/Be); Lonewolf Nunataks (LON) 94101, 50 (weathering grade Be) and Elephant Moraine (EET) 96029, 9 (weathering grade A/B). We also studied Murray sample BM1966, 48, P13114 which is a loan from the Natural History Museum in London. For the XCT work we used a centimetre-sized irregularly shaped sample of Murchison that was obtained commercially. It was embedded in resin and cut into a rectangular block of $9 \times 7 \times 6$ mm in size. The block was polished on three perpendicular faces to expose the sample surface and enable electron microscopy (Fig. 1). The face perpendicular to +z in Fig. 1 is hereafter referred to the +z side, the face perpendicular to +x is the +x side, and the face perpendicular to −y is the −y side. The +z side was chosen as the reference side, with the reference direction parallel to +y, as highlighted in Fig. 1.

2.2. BSE imaging, X-ray microanalyses and EBSD

Backscattered electron (BSE) imaging and qualitative X-ray analysis used a FEI Quanta 200F field emission environmental scanning electron microscope (SEM) operated at 20 kV. These techniques were used to characterise chondrules, the meteorite matrix, fractures and veins in all the samples, and to additionally determine the degree of alteration of three of the meteorites (EET 96029, LAP 031166 and MET 01072) with reference to the scheme of Rubin et al. (2007).

EBSD work was undertaken on calcite on three sides of the Murchison block, after polishing in colloidal silica, using an EDAX/TSL OIM 5.2 system attached to the Quanta SEM and equipped with a Hikari high speed camera. Kikuchi patterns were acquired with the stage tilted 70° towards the camera, and the standard hexagonal unit cell parameters for calcite were used for indexing: space group

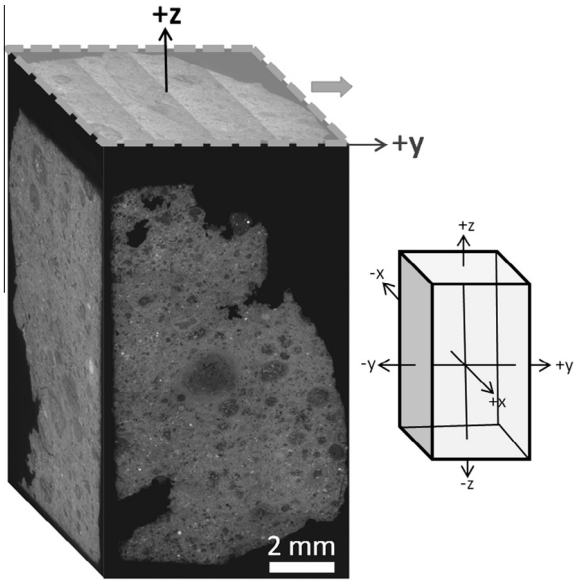

Fig. 1. SEM-BSE images of the three polished faces of the Murchison block embedded in resin (black). The orientation of the block is marked using x, y and z axes as shown in the schematic drawing. The reference side is the +z side highlighted in grey on the block, and the reference direction is marked by a grey thick arrow (along +y).

$R\bar{3}c$, $a = 0.499$ nm, $c = 0.1706$ nm. Indexing of Kikuchi patterns was optimized using the Hough transform with an interplanar angle tolerance of 2°. The binning was usually set to either 4×4 for a faster acquisition of a large area or 2×2 for more accurate indexing over a small area. The step size was set to between 0.1 and 2 μm depending on the size of the area to be analysed and the scale of the features of interest; i.e., a larger step size to detect calcite grains in the sample, and a smaller step size to map a twin boundary within a calcite grain. EBSD results are illustrated as orientation maps using the inverse pole figure (IPF) notation scheme, where each colour represents a particular crystallographic orientation. Pole figures showing the orientation of individual data points from different calcite grains in the sample were constructed using the TSL software. All the pole figures were plotted as stereographic projections in the upper hemisphere. EBSD maps were obtained from calcite grains on each of the three polished faces of the block. All of the analyses on one single side were carried out with the sample positioned with the same orientation in the SEM, so that the individual data points from that particular side could be compared in the same pole figure. In order to compare data points from all three perpendicular faces of the Murchison block, those points from the +x side and −y side were rotated in a stereonet to match the reference side and direction.

2.2.1. Calcite twin stress analysis

The crystallographic orientations of calcite grains and their respective *e*-twins as gathered from the EBSD work on the Murchison block were used for calcite twin stress analysis. This technique is widely applied to infer paleostress orientations in various terrestrial settings (Tourneret and Laurent, 1990; González-Casado and García-Cuevas, 1999; González-Casado et al., 2006; Schedl, 2006) and has also been successfully employed to explore stress relationships in a carbonaceous chondrite (Lindgren et al., 2011). Here, we used the classic *e*-twin stress analysis method of Turner (1953, 1962) to determine the orientation of the maximum compression (σ_1) that acted on the sample to form the calcite twins. This method is based on the fact that twins form in calcite during uniaxial compression (e.g., Spang, 1972; De Bresser and Spiers, 1997) and that there is a geometrical relationship between the pole to the twin plane, the host calcite *c*-axis, and the principal axes of stress (σ_1 and the maximum extension (σ_3)). By plotting the orientation of the *c*-axis and twin plane of each calcite grain on the same stereonet, the orientation of compression could be obtained as σ_1 lies 45° from the pole of the twin plane away from the *c*-axis of the host calcite (for more details, see Lindgren et al., 2011).

2.3. Transmission electron microscopy

For a more detailed examination of the calcite twins in Murchison, transmission electron microscopy (TEM) was performed on focused ion beam (FIB) foils of calcite grains. The sample was carbon coated prior to the FIB work. The foils were prepared using a FEI Nova 200 Dualbeam FIB instrument with 30 kV Ga^+ ions at a current ranging from 100 pA to 6 nA during different stages in foil milling. The foils were lifted out using the procedure of Lee et al. (2003) and welded with ion and electron beam deposited platinum on to the tines of a Cu holder. Diffraction contrast images and selected area electron diffraction (SAED) patterns were acquired using a FEI T20 TEM operated at 200 kV.

2.4. Aspect ratios and petrofabric analyses

The first step in petrofabric analysis was to determine the aspect ratios of chondrules, chondrule fragments and chondrule pseudomorphs, hereafter 'chondrules' for brevity. This work used BSE images of the seven thin sections and the three orthogonal faces of the Murchison block. Aspect ratios are expressed as the long axis of each chondrule divided by the diameter measured normal to the long axis and half way along its length (the same procedure as used in analysing the XCT data as described below). Note, the values obtained from thin sections are likely to be lower than the true aspect ratios of chondrules because the planes of the thin sections are unlikely to be oriented precisely parallel to the compression axis (where present). Most chondrules have a fine-grained rim and so the aspect ratio was determined both including and excluding the rim.

Petrofabrics were analysed using the technique of Rubin (2012), which is consistent with earlier studies (e.g., Tomeoka et al., 1999). The orientations of the long axes of all of the chondrules in the thin sections, and on the three faces of the Murchison block, were measured relative to the horizontal on the SEM monitor. From the spread of orientations in each dataset the median azimuth was calculated

and the angular deviation of each chondrule from this azimuth was plotted on a histogram. A tight clustering of measurements around the median azimuth indicates a strong petrofabric, and the degree of clustering is here expressed as the percent of chondrules that lie within 10° of the median (Rubin 2012). We also measured the orientations of open fractures, and veins of calcite, dolomite and gypsum. These plots are especially useful for investigating meteorite stress histories because Tomeoka et al. (1999) showed that chondrules are flattened in the plane of the shock front, and co-genetic fractures lie parallel and at a high angle to the shock front. It is important to be aware that in natural samples it can be difficult to know whether the fractures are pre- or post-terrestrial unless, for example, they are cross-cut by fusion crust as in the case of SCO 06043 (Lindgren et al., 2012).

2.5. High resolution XCT

High resolution XCT was performed on the Murchison block. It is a non-destructive imaging technique that enables 3D visualization and analysis of the internal structures and is therefore advantageous for rare and valuable samples such as meteorites (Ebel and Rivers, 2007). An XCT scan yields a 3D image in which greyscales represent X-ray attenuation, and has a first order dependence on density (Ketcham and Carlson, 2001). The sample is mounted on a stage with rotation axis perpendicular to the X-ray beam, and a series of 2D projections are collected at different angles as the sample is rotated. Each image therefore records a different mineral assembly along the beam path, and filtered back projection algorithms are used to reconstruct the 3D volume. XCT was performed using a Nikon Metris XT H 225 scanner at the Manchester X-ray Imaging Facility, University of Manchester, operated with a Cu target and an accelerating voltage of 120 kV and a 0.25 mm Cu filter to maximise the dynamic range. 2884 projections were collected with a 1 s exposure time. The resultant 3D volume has a voxel (3D pixel) resolution of 7.4 μm, and a modest built-in polynomial correction was applied to reduce the effect of beam hardening around the edge of the block. A 3D median filter (kernel of 3) was applied to the reconstructed image to reduce noise.

Petrographic analysis of the tomographic volume of the Murchison block follows the method of Hanna et al. (2012). The purpose of the present work was to measure the aspect ratios of chondrules and the petrofabric defined by chondrules in the XCT volume. Discernible objects with predominantly low X-ray attenuation (low CT numbers), which are described later to be chondrules, were delineated in the XCT images based on their greyscale values. Some of these dark-toned objects contained lighter toned (high CT number) cores. Numerous uniformly light-toned objects (high CT numbers) were also visible in the XCT data but were not segmented for the purpose of this study (as discussed later, these light-toned objects are mostly grains of sulphide or metal). Previous work has shown that the dark and light-toned objects in XCT scans of Murchison display different deformation trends, with the dark-toned objects typically showing a stronger degree of preferred orientation (Hanna et al., 2012). The range of greyscale values of the individual objects often overlapped with the greyscale values of the surrounding matrix, making routine automatic segmentation algorithms unsuitable. Therefore all dark-toned objects (with or without lighter cores) were manually segmented using the Avizo™ software by delineating one or more cross sections in each orthogonal plane. The segmented data were then imported into the Blob3D program (Ketcham, 2005a,b) that fitted an ellipsoid to the shape suggested by the 3 (or more) orthogonal planes and extracted size, shape, and orientation information for the segmented objects.

3. RESULTS

3.1. Aspect ratio and petrofabric analyses of chondrules in 2D

The chondrules that were analysed in each meteorite have a considerable range of aspect ratios, and to be consistent with previous work (Tomeoka et al., 1999), the mean and standard deviation of each dataset is quoted. A double-blind test on chondrules in QUE 93005 (Fig. 2a; a flattened chondrule where the mafic silicates are completely replaced by phyllosilicates) by two of the authors found excellent agree-

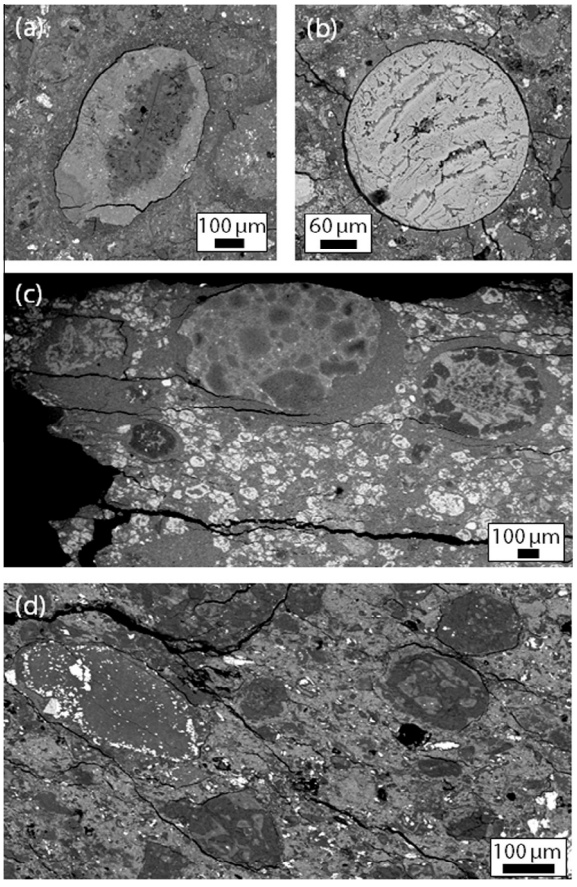

Fig. 2. SEM-BSE images of chondrules in (a) QUE 93005, (b) EET 96029, (c) MET 01072 and chondrule pseudomorphs in (d) SCO 06043. Note fractures in (c) and (d).

ment in aspect ratio measurements: 1.35 ± 0.27 ($n = 21$; Lindgren) and 1.37 ± 0.31 ($n = 18$; Lee). The aspect ratios of most chondrules are lower (i.e., closer to 1) if the rim is included in the measurements. Out of all the rimmed chondrules studied the average aspect ratio is 1.42 including rim and 1.51 excluding rim. Note that most of the discussion of data from the present study uses aspect ratios excluding rims in order to be consistent with XCT data from Murchison, where the rims could not be reliably distinguished from the matrix. Some chondrules examined in the present study are intact and circular in cross-section (i.e., aspect ratio of 1; Fig. 2b; a barred olivine chondrule), in particular the chondrules with barred and cryptocrystalline textures, whereas the majority of the porphyritic chondrules have irregular shapes with aspect ratios greater than 1. In some of the thin sections the petrofabric is particularly strongly developed (Fig. 2c, d).

3.1.1. Thin sections

EET 96029 has here been classified as a CM2.5. It is the least altered meteorite used in the present study and is unusual among the CMs for containing at least one chondrule that retains mesostasis glass (Lindgren and Lee, 2014), and many of the other chondrules have been minimally aqueously altered. Chondrules range in diameter from ~0.3 to 1.0 mm, have a mean aspect ratio of 1.30 ± 0.25 ($n = 20$), and there is no evidence of a petrofabric (15% of chondrule long axes within 10° of the median azimuth; Table 2, Fig. 3a). No veins or fractures were found.

Murray (CM2.4–2.5) is a relatively weakly altered CM chondrite. The mineralogy and microstructure of the thin section used here was described by Lee and Ellen (2008). The chondrules range in diameter from ~0.1 to 1.0 mm, their mean aspect ratio is 1.28 ± 0.27 ($n = 23$), and there is little indication of a petrofabric (13% of chondrule long axes within 10° of the median azimuth; Table 2, Fig. 3b). No veins or fractures were found. Rubin (2012) likewise showed that Murray lacks a petrofabric (18% of particle long axes within 10° of the median azimuth).

LON 94101 (CM2.3) has many chondrules with preserved ferromagnesian silicates, but some are partially altered to calcite and/or phyllosilicate (Lee et al., 2013, 2014). The mineralogy and microstructure of the thin section used in the present study has been described previously by Lindgren et al. (2011) and Lee et al. (2013). The chondrules range in diameter from ~0.1 to 0.6 mm, their mean aspect ratio is 1.29 ± 0.19 ($n = 21$), and they define a weak petrofabric (33% of chondrule long axes within 10° of the median azimuth; Table 2, Fig. 3c). The sample also contains a ~1 mm long and 70–130 μm wide calcite vein (Lindgren et al., 2011), which is oriented at a high angle to the petrofabric (Fig. 3c). The calcite vein has a fine-scale contortion. LON 94101 has been shown to contain a wide range of clasts with different lithologies (e.g., Lindgren et al., 2013a) each of which could have a different petrofabric.

MET 01072 has here been classified to a CM2.3 based on the extent of alteration of mafic silicate phenocrysts in chondrules. Ferromagnesian silicates are present in the chondrules, but have been partially altered to phyllosilicate. The chondrules have broad fine-grained rims and some of them contain inclusions of Fe–Ni metal and sulphides. The chondrules range in diameter from ~0.1 to 0.8 mm and their mean aspect ratio is 1.84 ± 0.52 ($n = 45$) (Table 2, Fig. 3d). Flattening and elongation of the chondrules in a common direction gives the sample a strong petrofabric (Nakamura et al., 2012). The present study measured 78% of chondrule long axes within 10° of the median azimuth, giving it the strongest petrofabric of the sample suite. This thin section also contains well-developed fractures, 5–20 μm wide, in the same plane as chondrule alignment and 10–60 μm wide fractures oriented normal to the chondrule petrofabric (Fig. 2c).

QUE 93005 (CM2.1) has highly altered chondrules (Fig. 2b) in a matrix that contains abundant carbonates (Rubin et al., 2007; de Leuw et al., 2010; Lee et al., 2012; Velbel et al., 2013). The chondrules range in diameter from ~0.1 to 1.2 mm, they have a mean aspect ratio of

Table 2
Chondrule mean 2D aspect ratios associated petrofabrics in the CM meteorites.

Meteorite	Petrologic subtype[b]	Including rim		n[c]	Excluding rim		n[c]	Petrofabric[d]
		Aspect ratio	1σ		Aspect ratio	1σ		
Murchison block	2.5							
+x side		1.50	0.42	10	1.67	0.51	20	50
−y side		1.38	0.23	10	1.54	0.30	20	40
+z side		1.15	0.11	11	1.24	0.22	20	20
EET 96029	2.5	1.20	0.21	20	1.30	0.25	20	15
Murray	2.45	1.29	0.24	23	1.28	0.27	23	13
LON 94101	2.3	1.27	0.12	21	1.29	0.19	21	33
MET 01072	2.3	1.68	0.44	41	1.84	0.52	45	78
QUE 93005	2.1	1.28	0.25	11	1.35	0.27	20	43
LAP 031166	2.1	1.44	0.25	20	1.57	0.36	20	70
SCO 06043[a]	2.0	1.97	0.46	23	1.97	0.46	23	57

[a] Fine-grained rims, if present, cannot be distinguished from the chondrule pseudomorphs.
[b] After Rubin et al. (2007).
[c] Number of chondrules analysed.
[d] Percent chondrules with their long axes within 10° of the median azimuth.

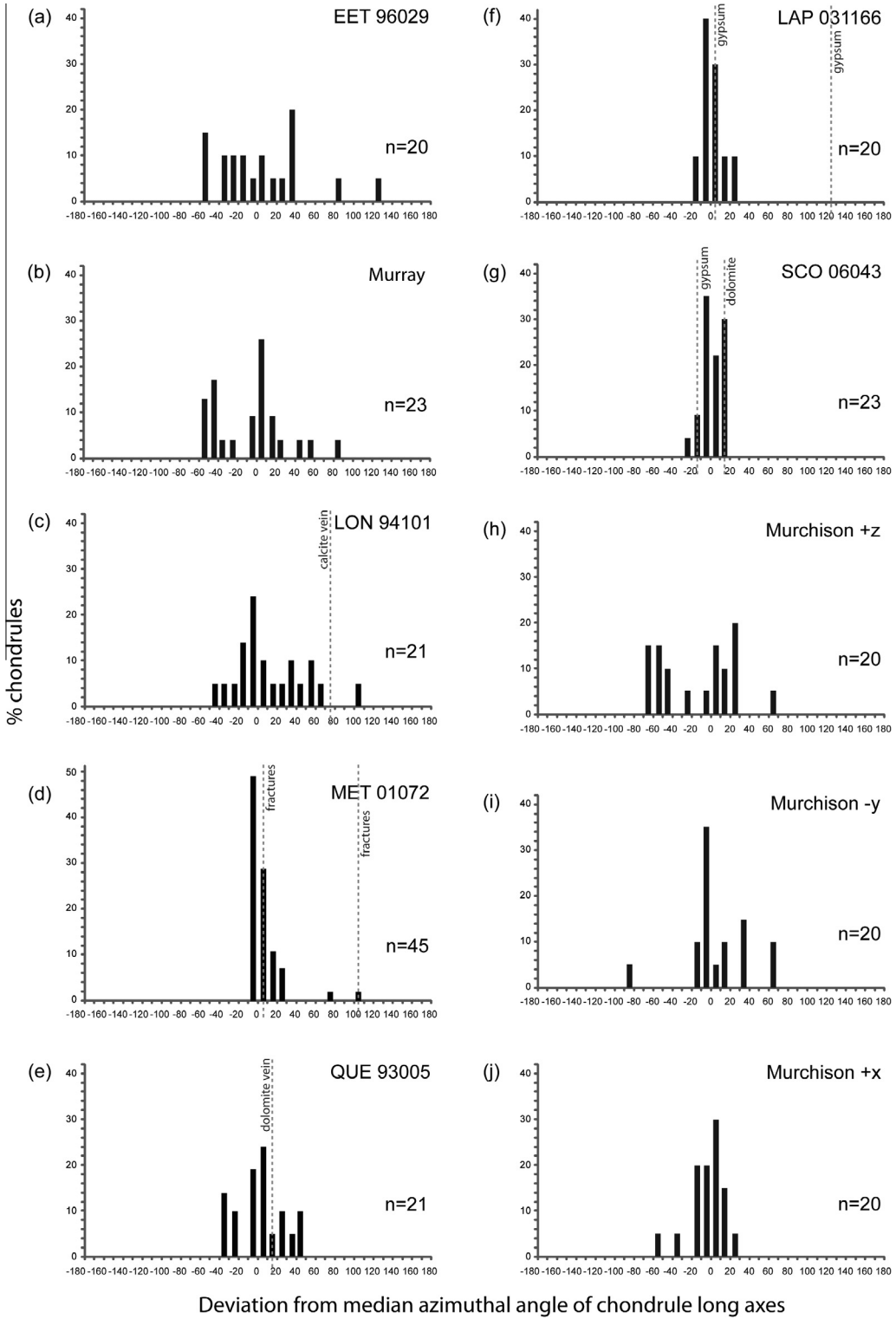

Fig. 3. Histograms showing the deviation of the long axes of chondrules in 7 CM thin sections from their median azimuthal angle; (a) EET 96029, (b) Murray, (c) LON 94101, (d) MET 01072, (e) QUE 93005, (f) LAP 031166, and (g) SCO 06043. Data for the three faces of the Murchison block are also shown in (h) side +z, (i) side −y, (j) side +x. Sharp peaks in the histograms indicate strong petrofabrics. The orientations of fractures and veins (calcite, dolomite or gypsum) in the thin sections, relative to the median azimuthal angle of the long axes of chondrules, are indicated by dashed lines.

1.35 ± 0.27 ($n = 21$) and define a moderate petrofabric (43% of chondrule long axes within 10° of the median azimuth; Table 2, Fig. 3e). Rubin (2012) found a slightly weaker petrofabric in QUE 93005 defined by particles including chondrules (32% of particle long axes within 10° of the median azimuth). The QUE 93005 thin section examined here contains an irregular 0.6 mm long dolomite vein, with a width of 20–100 μm, oriented in the same plane as the petrofabric (Fig. 3e). The matrix carbonates contain coarse polymineralic grains that have been broken by fracturing, which may have taken place during fluidisation of the matrix accompanying degassing, or during impact brecciation (Lee et al., 2012).

LAP 031166 has here been classified to a CM2.1 based on the extent of chondrule alteration. Many chondrules are composed of phyllosilicate or calcite, i.e., they are pseudomorphs (Lee et al., 2014), but in some of them ferromagnesian silicates are preserved. Sulphides occur along the rims and in the interiors of chondrules. The chondrules range in diameter from ~0.2 to 1.4 mm. Fine-grained rims are relatively thin in this sample and are most prominent on the least altered chondrules. The chondrules are flattened with a mean aspect ratio of 1.57 ± 0.36 ($n = 20$) and they define a strong petrofabric (70% of chondrule long axes within 10° of the median azimuth; Table 2, Fig. 3f). The thin section contains two sets of fractures: parallel and at right angles to the defined petrofabric. The fractures are 5–30 μm wide and are partially filled with gypsum.

SCO 06043 (CM2.0) is the most highly aqueously altered of the studied meteorites. All of the chondrules have been completely altered to phyllosilicate, with rims and inclusions of sulphides occurring in some of them. The chondrules range in diameter from 0.1 to 0.4 mm. Fine-grained rims, if present, cannot be distinguished from the chondrule pseudomorphs. The chondrules are flattened with a high mean aspect ratio of 1.97 ± 0.46 ($n = 23$). They are elongated in a common direction to give the sample a strong petrofabric (57% of chondrule long axes within 10° of the median azimuth; Table 2, Figs. 3g, 2d). This sample also contains several ~10 μm wide veins of dolomite that are cross-cut by its fusion crust (Lindgren et al., 2012). These dolomite veins lie sub-parallel to the petrofabric. In addition to dolomite veins, 5–30 μm wide fractures partially filled with gypsum and iron oxide occur, also sub-parallel to the petrofabric but with a different orientation (Fig. 3g).

3.1.2. Murchison block

Murchison (CM2.5, Fig. 3h, i, j) has undergone relatively mild aqueous alteration. Its properties are described here in more detail than the other CMs in order to help interpret the XCT and EBSD data. Most of the chondrules in Murchison range in diameter from ~0.1 to 0.5 mm; with a few at larger diameters of ~1.0 to 1.5 mm. Fine grained rims are common. The chondrules generally display a porphyritic texture with unaltered ferromagnesian silicates, but the mesostasis and some phenocrysts have been altered to phyllosilicate. Some chondrules contain Fe–Ni metal grains in their cores. The matrix is fine-grained and composed of phyllosilicate and tochilinite-phyllosilicate intergrowths, and also contains grains of Fe–Ni metal, sulphide and unaltered ferromagnesian silicates. Ca-carbonate grains are scattered throughout the matrix; most are calcite but a few grains of aragonite were also detected using EBSD. The aragonite grains are small; ⩽20 μm in diameter and have acicular shape (Lee et al., 2014). The calcite grains have rounded, subhedral or irregular crystal shapes, and range in size from ~10 to 80 μm. They sometimes contain inclusions of, or are rimmed by, tochilinite or tochilinite-phyllosilicate intergrowths (Fig. 4a, b). The calcite occurs mainly as isolated grains, but in a few places clusters of grains are observed (Fig. 4c). Some calcite grains display a zonation, enhanced by high concentrations of pores with diameters of around 200 nm (Fig. 4d). Twinned calcite grains were used for the *e*-twin stress analyses (see below).

There are significant differences in chondrule aspect ratio and petrofabrics between the three faces of the Murchison block. Chondrules exposed on the +z side have the lowest mean aspect ratio (1.24 ± 0.22, $n = 20$) and a correspondingly weak petrofabric (20% of chondrule long axes within 10° of the median azimuth; Table 2, Fig. 3h). The −y side chondrules are more flattened (mean aspect ratio of 1.54 ± 0.30; $n = 20$) and define a stronger petrofabric (40% of chondrule long axes within 10° of the median azimuth; Table 2, Fig. 3i). The chondrules with the greatest mean aspect ratio are on the +x side (1.67 ± 0.51; $n = 20$) which also has the strongest petrofabric (50% of chondrule long axes within 10° of the median azimuth; Table 2, Fig. 3j). Rubin (2012) also examined Murchison and found that 17% of particle long axes within 10° of the median azimuth, which is close to the weakest petrofabric recorded (on the +z side of the block).

3.1.3. Correlation between aspect ratio, petrofabric and petrologic subtype

Compilation of data from thin sections and the three faces of the Murchison block demonstrates that the chondrule aspect ratio and strength of petrofabric are reasonably well correlated ($r^2 = 0.65$; Fig. 5a). In addition, there is a weaker anticorrelation between petrofabric and petrologic subtype ($r^2 = 0.35$; Fig. 5b; where an r^2 value of 1 represents a perfect fit). The variation in values between the three faces of the Murchison block highlights the influence of the orientation of the thin section for measuring and interpreting aspect ratio and petrofabric.

3.1.4. Calcite e-twin stress analysis

SEM and EBSD results confirm that calcite grains throughout Murchison contain twins that are present mostly in one (Fig. 6a), sometimes two (Fig. 6b), and in rare cases three orientations. In one of the calcite grains with two sets of twins, one set is cross-cut and offset by a later set (Fig. 6b). EBSD confirms that the twins are *e*-twins, i.e., their composition planes are parallel to $\{\bar{1}018\}$ and they have a misorientation angle of 78° to the host calcite (see Burkhard, 1993 for a review). In addition to *e*-twins, $f = \{\bar{1}012\}$ and $r = \{10\bar{1}4\}$ planes of slip can also be activated in calcite by stress (Barber and Wenk, 1979; De Bresser and Spiers, 1997), but none were observed in this study. The calcite twins in this sample are straight and usually ~1 to 2 μm thick with a spacing of 1–4 μm. Stress anal-

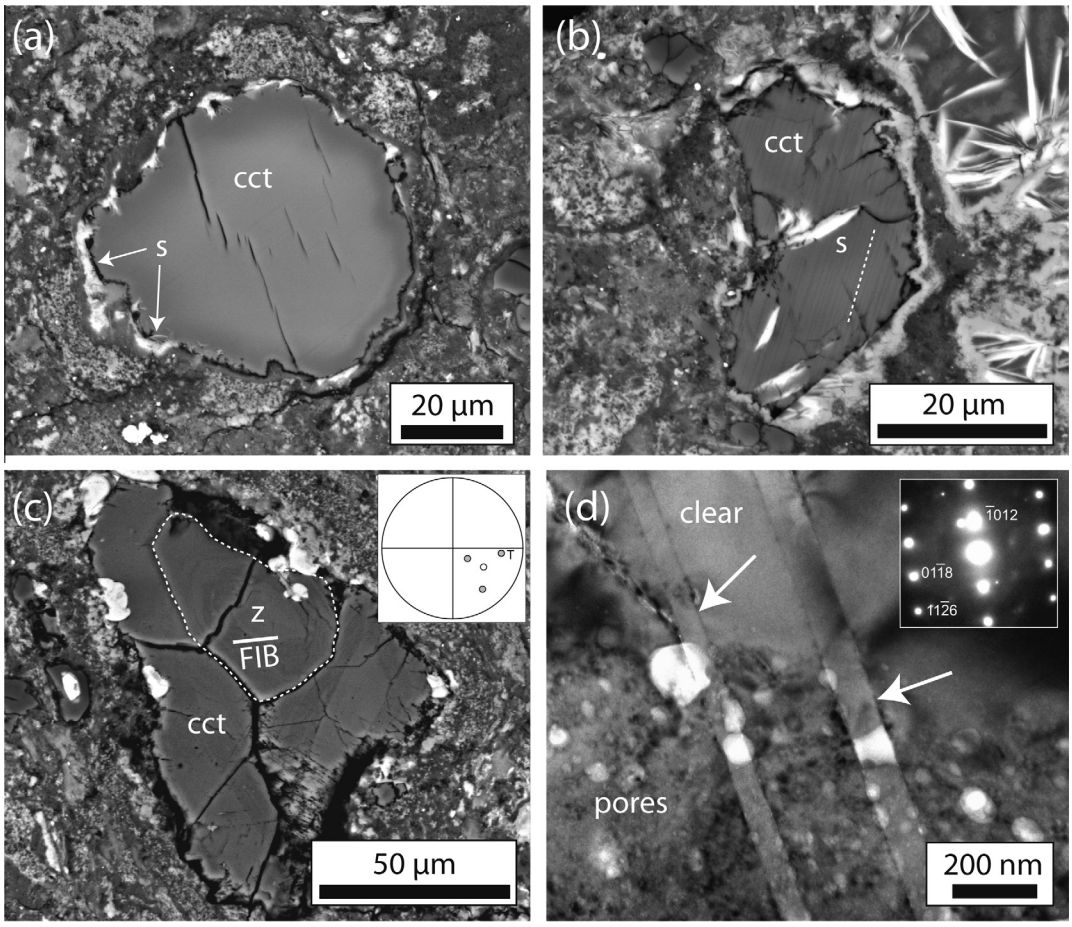

Fig. 4. Images of calcite from the +x side of the Murchison block. (a) SEM-BSE image of an anhedral calcite grain (cct) partially rimmed by sulphides (s). (b) SEM-BSE image of a subhedral calcite grain (cct) with inclusions of sulphides (s). Twinning is observed and the twin orientation is outlined with a dashed white line. (c) SEM-BSE image of a cluster of calcite crystals where some grains (dashed white line) show a zonation (z). The inset EBSD pole figure is from the zoned grain. The open circle is the pole to (0001) whereas the grey circles are the poles to $\{\bar{1}018\}$. T marks the orientation of the twins observed in this grain by EBSD and TEM. The white solid line 'FIB' shows the location of where a FIB foil was extracted. (d) Bright-field diffraction contrast TEM image of the FIB foil located in (c) showing that the zonation in the calcite grain is caused by a sharp transition from clear calcite to calcite with a high concentration of pores. White arrows point to *e*-twin planes. The inset $[4\bar{6}21]$ SAED pattern shows that the twin composition planes are parallel to $(01\bar{1}8)$.

ysis was carried out on 23 calcite grains with one visible twin plane (7 grains on the +x side, 7 grains on the +y side and 9 grains on the +z side) and the orientations of σ_1 for these grains, i.e., $\sigma_{1calcite}$, are plotted on the pole figures in Fig. 7a and b. The orientations of $\sigma_{1calcite}$ are somewhat scattered, although a weak clustering occurs in two or three areas of the projection, indicating that $\sigma_{1calcite}$ is inclined at fairly high angles to the reference side of the block (Fig. 1).

3.2. XCT analyses of the Murchison block

3.2.1. Identity of XCT objects

Comparison between the SEM observations of the three polished sides of the Murchison block and the XCT data confirm that most of the dark-toned objects in the XCT volume are chondrules (Fig. 8a, b). In the XCT volume they range in size from ~0.1 to 2.0 mm. Most of the chondrules are darker in the XCT volume than the slightly lighter toned (i.e., denser) fine-grained phyllosilicate-sulphide matrix, with exception for the chondrules that contain metal and sulphide grains. These grains often appear brighter in the interiors of chondrules. Other bright phases in the XCT volume are isolated metal or sulphide grains that are scattered in the matrix. It is also possible that some of the dark-toned XCT objects could be highly altered CM materials, which have previously been reported in Murchison (Fuchs et al., 1973; Olsen et al., 1988). However, only one such clast (~50 µm in diameter) was observed by SEM imaging and so these clasts are likely to comprise a very small proportion of the 133 dark-toned XCT objects analysed. It is also possible that some of the smaller dark objects could be calcite grains, which have a lower density than the matrix. However, the largest calcite grain observed by SEM was ~80 µm in diameter, and only 10 of 133 dark-toned objects are equal to or smaller than this length in cross-section. Therefore, it is most likely that the majority of the XCT dark-toned objects represent chondrules, which are composed of (i) ferromagnesian silicates with more or less altered mesostasis, (ii) ferromagnesian silicates with altered mesostasis and interspersed Fe–Ni metal grains, or

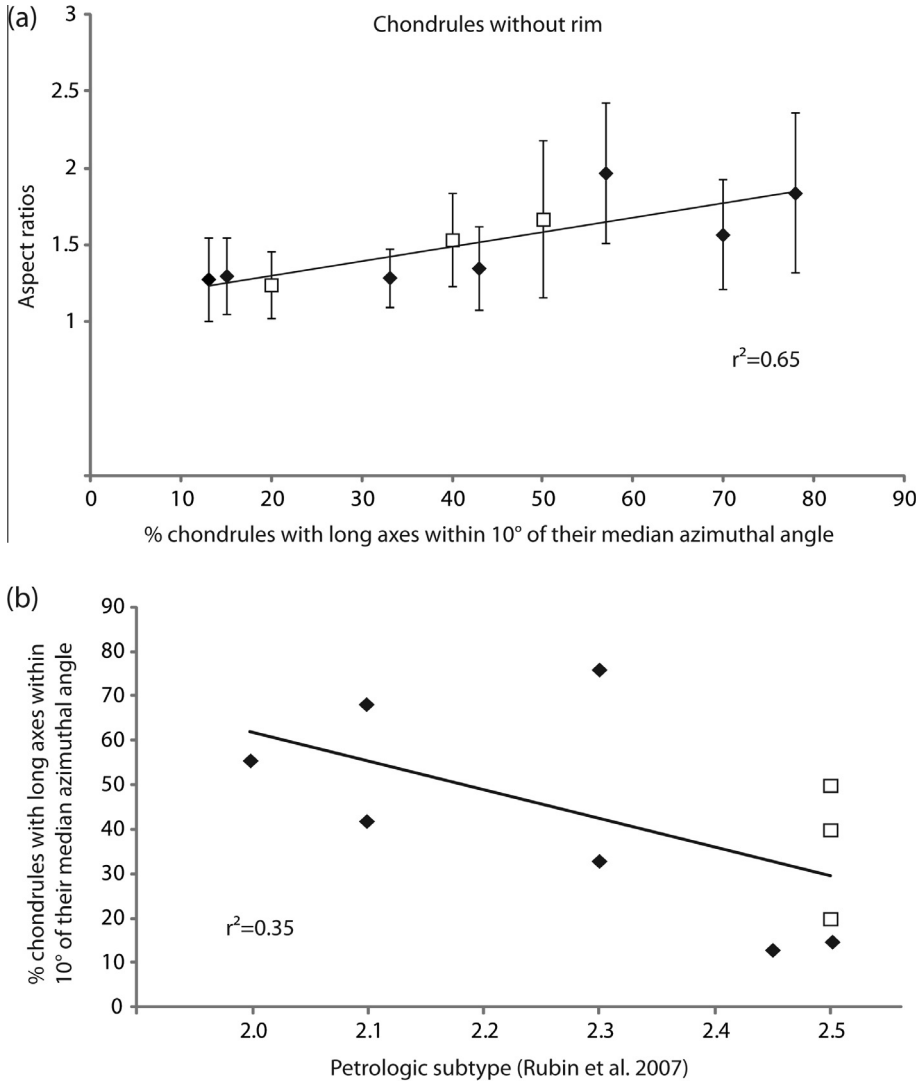

Fig. 5. Cross-plots of data from Table 2. The black diamonds are thin sections, and open squares are the three faces of the Murchison block. (a) Aspect ratio of chondrules *vs* the petrofabric defined by them, showing that with higher aspect ratio a stronger petrofabric is present. (b) The petrofabric defined by chondrules *vs* the petrologic subtype of their host meteorite, showing a stronger petrofabric with increasing degree of aqueous alteration.

(iii) ferromagnesian silicates partially altered to phyllosilicates with altered mesostasis (Fig. 8a, b).

3.2.2. Chondrule orientation analysis

The 133 dark-toned XCT objects, hereafter 'chondrules', were segmented and their best-fit ellipsoid orientations plotted on stereonets to assess the degree and orientation of their preferred alignment (Fig. 7c, d). Using the definitions and methods of Woodcock (1977) and Woodcock and Naylor (1983), the primary (longest) ellipsoid axes orientations have a girdle distribution (shape parameter $K = 0.046$) (Fig. 7c) and the tertiary (shortest) ellipsoid axes are clustered $K = 2.428$) (Fig. 7d); both distributions are non-random at the 99% confidence interval. The girdle distribution of the primary axes combined with the clustering of the tertiary axes is consistent with a foliation fabric, rather than a lineation (Turner and Weiss, 1963). The foliation fabric strength as defined by the strength parameter '*C*' of Woodcock and Naylor (1983) is 'moderately weak' with $C = 1.46$ and $C = 1.92$ for the primary and tertiary axes respectively. The strong clustering of the chondrules tertiary axes is consistent with a single preferred orientation of maximum compression, i.e., $\sigma_{1chondrule}$ that is semi-vertical to the reference side of the Murchison block (Fig. 1). However, the girdle distribution of the chondrule primary axes shows that, although all oriented within the same plane, the chondrule long axes are oriented in multiple directions within this plane. The shapes of the chondrule best-fit ellipsoids were analysed by plotting them on a Sneed and Folk ternary diagram (Sneed and Folk, 1958; Graham and Midgley, 2000) (Fig. 9). Results indicate that the majority (84%) have a significantly non-compact (non-spherical) shape and that they tend to be elongated (i.e., non-platy) in shape. Although the elongated shape

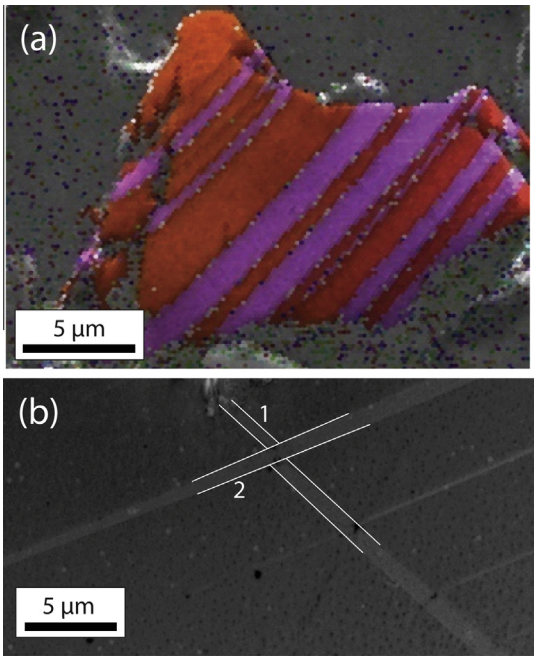

Fig. 6. Calcite twinning from the −y side of the Murchison block. (a) IPF coloured EBSD orientation map of a calcite grain with one set of *e*-twins. (b) SEM-BSE image of a calcite grain with two sets of *e*-twins partially outlined by white lines where an earlier twin set (1) is cross-cut and offset by a later set of twins (2). (For interpretation of the references to colour in this figure legend, the reader is referred to the web version of this article.)

of the chondrules suggest that a lineation may be present, their longest axes are not preferentially orientated in a cluster distribution (Fig. 7c) as would be expected for a lineation fabric. The aspect ratio of the best-fit ellipsoid for each chondrule in the segmented population has a mean of 1.75 ± 0.39 ($n = 133$). These XCT results are in excellent agreement with the aspect ratios of chondrules on the +x side of the block (1.67 ± 0.51).

4. DISCUSSION

4.1. Aspect ratios and petrofabric analysed in 2D *vs* 3D

Most of the aspect ratio and petrofabric measurements reported here and in previous studies of CM deformation (Lee and Ellen, 2008; Rubin, 2012) have used thin sections. The 2D surfaces of thin sections not specially prepared for paleostress analyses are unlikely to be oriented so that they record the maximum aspect ratios and strongest petrofabrics (i.e., not normal to the shock wave). This constraint is highlighted by our data from the 3 sides of the Murchison block, which show mean aspect ratios ranging from 1.24 to 1.67. On the other hand, aspect ratios and petrofabrics quantified by XCT will be true values, and indeed the aspect ratio for Murchison chondrules measured by XCT (1.75) is close to the maximum value derived from SEM images of the polished block (i.e., +x side, 1.67). However, the main disadvantage of XCT is that the segmented objects cannot be unambiguously identified; whilst we are confident that most of the dark toned XCT objects that were segmented from the Murchison dataset are chondrules, it is possible that some were clasts or large calcite grains. In addition, the type of chondrule cannot be determined from the XCT data, and those with fayalitic compositions may not be detectable next to the meteorite matrix.

4.2. Evidence for petrofabrics and their origins

Results of this study add to the evidence from previous work that many CMs have a petrofabric (Table 1). It may be defined by the common alignment of chondrules, but petrofabrics can also be recognised by the preferred orientation of a variety of other mineral grains and phyllosilicate-rich aggregates that are part of the fine-grained meteorite matrix (Table 1). In order to answer our question of how these petrofabrics form (i.e., lithostatic compaction *vs* attenuated high intensity shock events *vs* multiple low intensity events), it is necessary to establish the reasons for deformation of chondrules and the matrix. From an understanding of petrofabric formation we can then explore the broader implications for understanding the histories of CM carbonaceous chondrites.

4.3. Chondrule flattening in ordinary and CV chondrites

Chondrule flattening and associated petrofabrics were first recognised and studied in ordinary chondrites (e.g., Dodd, 1965; Martin and Mills, 1980; Sneyd et al., 1988; Gattacceca et al., 2005; Rubin and Swindle, 2011) and the CV3 carbonaceous chondrites (e.g., Martin et al., 1975; Cain et al., 1986; Scott et al., 1992; Nakamura et al., 2000; Gattacceca et al., 2005; Table 1). This previous work has been based mainly on images of chondrules in thin section or on two or more mutually perpendicular faces of polished blocks, but AMS (anisotropy of magnetic susceptibility) has also been used to detect petrofabrics formed by the preferred orientation of metal grains (Sneyd et al., 1988; Gattacceca et al., 2005). Most of these studies have shown that flattened chondrules together define a foliation, and some have also found evidence for a weak lineation (e.g., Dodd, 1965; Sneyd et al., 1988). Suggested explanations for the chondrule flattening and petrofabrics have evolved from deposition (Dodd, 1965), through lithostatic compaction (Martin and Mills, 1980; Cain et al., 1986) to shock (Sneyd et al., 1988; Scott et al., 1992; Gattacceca et al., 2005). This latter hypothesis has been supported by the good correspondence between the shock stages of naturally deformed CV3s and aspect ratios of their chondrules (Scott et al., 1992; Fig. 10), and by the fact that flattened chondrules have been formed by shock-recovery experiments on Allende (CV3) (Nakamura et al., 1995, 2000). The threshold pressure between undeformed and flattened chondrules in naturally and experimentally shocked CV3 meteorites is ~10 GPa (Fig. 10).

4.4. Chondrule flattening in CM chondrites

Tomeoka et al. (1999) undertook shock-recovery experiments on Murchison, and in common with the work by

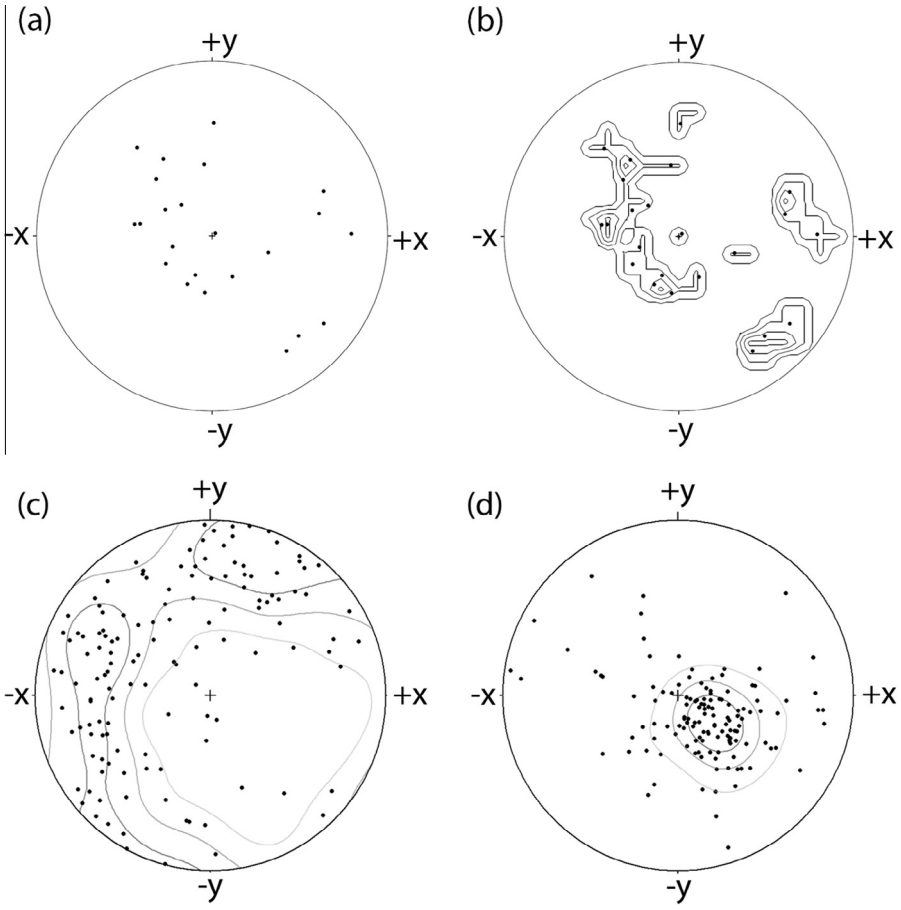

Fig. 7. Stress orientation data from the Murchison block. The plots are oriented relative to the block as shown in Fig. 1. (a) Pole figure showing the orientations of σ_1 for 23 calcite grains (i.e., $\sigma_{1calcite}$) as gathered from EBSD and calcite twin stress analyses. (b) An area% contoured plot of (a) produced in Stereonet9 (http://www.geo.cornell.edu/geology/faculty/RWA/programs/stereonet.html). (c) Stereonet plot of the longest (primary) axes of best fit ellipsoids to 133 segmented XCT chondrules. (d) Stereonet plot of the shortest (tertiary) axes of best fit ellipsoids to 133 segmented XCT chondrules (i.e., $\sigma_{1chondrule}$). The stereonet plots in (c) and (d) are produced with Stereo32 software, and the density contour intervals are drawn using cosine sums; max density for (c) is 17.6 and (d) is 36.7.

Nakamura et al. (2000) on Allende, showed that the CM chondrules are flattened by shock. The threshold pressure between undeformed Murchison chondrules and those with a measurable flattening lies at between 4 and 10 GPa (i.e., within shock stage S2), which is similar to the threshold for chondrule deformation in the CVs (Fig. 10). Thus, one explanation for flattening of chondrules in the CM2s is that these meteorites were shocked once and to a minimum pressure of 4 GPa.

4.4.1. Initial aspect ratios of CM chondrules

In order to confidently use the aspect ratio data to investigate the magnitude of compaction, the nature of chondrules prior to compaction should be evaluated. A proportion of the range of aspect ratios of chondrules in each meteorite will reflect the presence of chondrules with different initial (pre-compaction) aspect ratios, i.e., chondrules with barred and cryptocrystalline textures tend to be more circular than the porphyritic chondrules (e.g., Nelson and Rubin, 2002). Thus, the mean initial aspect ratio of chondrules in each CM must have been greater than 1. This value can be estimated using results from the Murchison block. Although the Murchison chondrules have undergone significant flattening, determination of $\sigma_{1calcite}$ and $\sigma_{1chondrule}$ show that deformation of the block was largely in response to uniaxial compaction, albeit in several events (see discussion below). Therefore chondrules exposed on the +z side of the block will show least flattening, and their mean aspect ratio (1.24 ± 0.22) is likely to be close to the initial value. An aspect ratio of 1.24 is similar to that of chondrules in Murchison (1.17 ± 0.13) measured by Tomeoka et al. (1999) prior to their impact experiments. We therefore suggest that the population of chondrules in each of the CM samples studied here had an initial aspect ratio of ~1.2, so that a mean in excess of that value is interpreted to reflect compaction.

4.4.2. Pressures indicated by chondrule flattening

The empirical relationships between aspect ratio and shock pressure that were determined by Tomeoka et al. (1999) and Nakamura et al. (2000) can be used to estimate the magnitude of a *single* shock event that would be

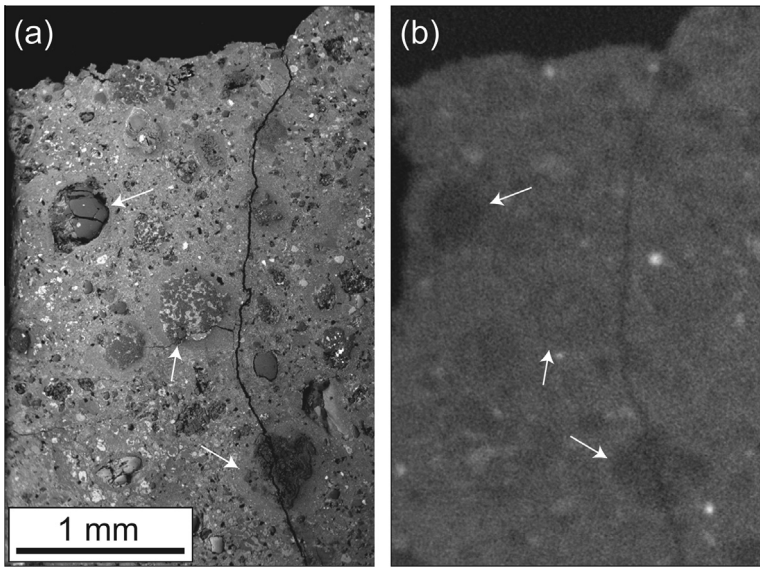

Fig. 8. Images from the reference side of the Murchison block. (a) SEM-BSE image with arrows pointing to some of the chondrules. (b) The appearance of the same chondrules as dark-toned objects in a closely corresponding XCT slice. Darkest greyscales represent the least dense phases in the block, while lighter greyscales represent denser material. For orientation, note the fracture running across both images. The white specks are grains of sulphide and/or metal.

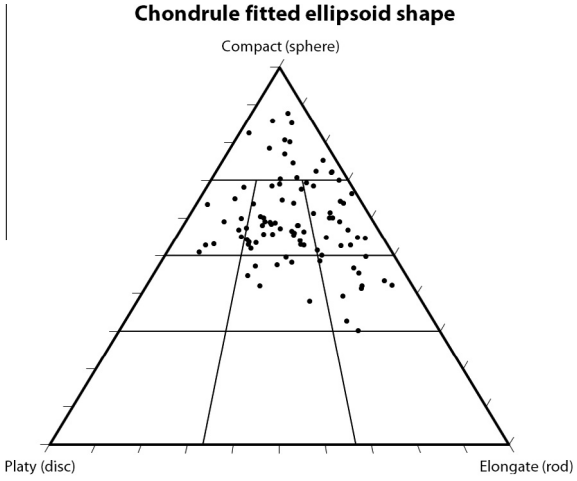

Fig. 9. XCT data from the Murchison block with chondrule best-fit ellipsoid shapes plotted on a Sneed and Folk (1958) ternary diagram using TRI-PLOT software (Graham and Midgley, 2000). The ellipsoid axis lengths are used to plot each chondrule shape within the triangle whose apices represent the idealized particle shapes indicated. Most of the chondrules are non-compact (non-spherical) and tend to be elongate (more rod-like) in shape.

required to flatten chondrules to the degrees observed in this study. Experimental work shows that there is a limit to the degree of flattening of chondrules caused by *single* impact shock (e.g., Tomeoka et al., 1999). We recognise that these experiments may be imperfect analogues of conditions within parent bodies during hypervelocity impact, but the correspondence between the threshold pressure for chondrule flattening in naturally shocked and experimentally shocked CVs (Fig. 10) gives us confidence in our approach. A significant question is whether shock came before, during or after aqueous alteration of the matrix and chondrules, and Fig. 10 shows that for a given shock pressure chondrules are flatter in Allende than Murchison. As Allende is largely anhydrous, it may be somewhat similar to a hypothetical CM3 meteorite to be used to indicate pre-alteration response of a CM to shock. However, some caution should be taken in this comparison since Allende is a CV chondrite with a smaller proportion of matrix and larger sized chondrules compared to the CM chondrite Murchison; this difference could also have had an effect on the distribution of the shock wave energy. Differences between Allende and Murchison in their relationship of aspect ratio to shock (Fig. 10), are most likely because the phyllosilicate-rich and microporous matrix of Murchison attenuates shock waves more effectively than the matrix of Allende. Therefore, in Table 3 we have used aspect ratios of chondrules in the eight CMs to estimate magnitudes of single shock events that could have produced flattening (where present) using the calibrations of both Tomeoka et al. (1999; possibly representative of post-alteration shock) and Nakamura et al. (2000; possibly representative of pre-alteration shock).

4.5. Other indicators of shock pressure

The data in Table 3 show the pressures required to generate the observed aspect ratios in *single* impacts are considerably higher than indicated by the shock stages of the individual meteorites (where available). Given that most CMs are breccias, the mismatch between shock pressures inferred by comparison with the experimental results and those indicated by olivine microstructures may just be due to intra-meteorite heterogeneities (i.e., the samples used in the present study are from parts of the meteorites that are more highly shocked than previous studies). Therefore we

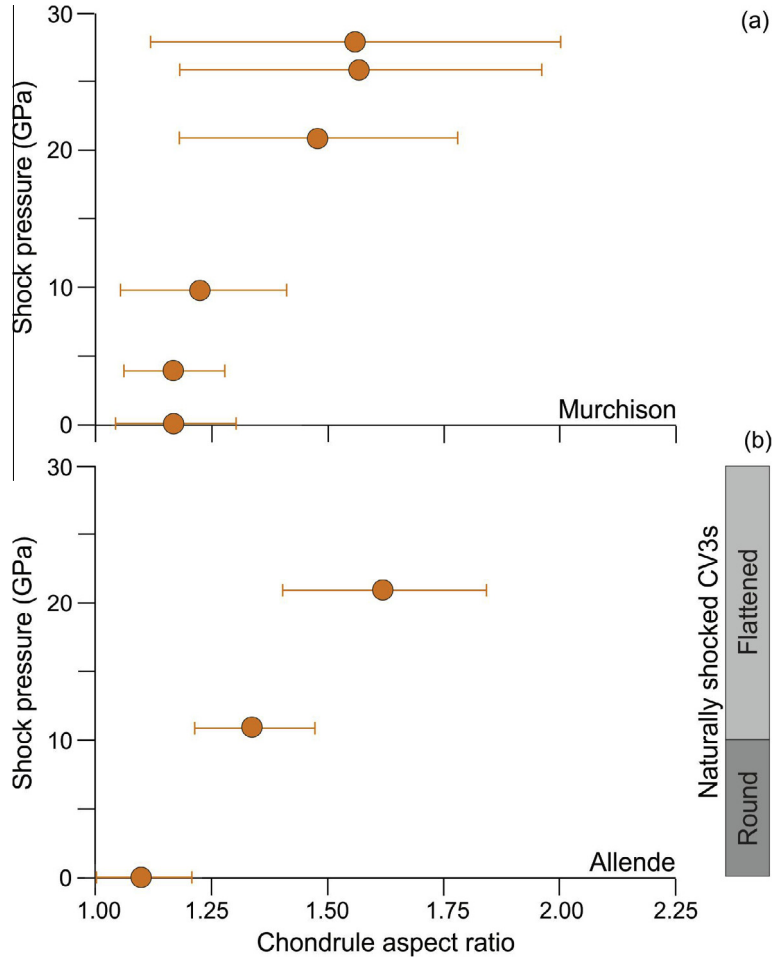

Fig. 10. Plots of the correspondence between shock pressure and chondrule aspect ratio. (a) Data from shock-recovery experiments using Murchison (CM2.5; Tomeoka et al., 1999). (b) Data from shock-recovery experiments using Allende (CV3; Nakamura et al., 2000). The column on the right hand side of this graph shows the pressures recorded by naturally shocked CV3 meteorites that contain round or flattened chondrules (from Scott et al., 1992).

Table 3
Indicators of impacts in the CM meteorites studied.

Meteorite	Petrologic subtype[a]	Shock pressure inferred from chondrule aspect ratio (GPa)[b]	Shock stage	Veins/fractures present?
SCO 06043	2.0	>30	nd	Yes
MET 01072	2.3	29 to >30	nd	Yes
Murchison XCT	2.5	24 to >30	S1[c,d]/S1–S2[e]	No
Murchison +x side	2.5	22 to >30	S1[c,d]/S1–S2[e]	No
LAP 031166	2.1	18–28	nd	Yes
QUE 93005	2.1	9–12	S1[c]	Yes
LON 94101	2.3	7–9	nd	Yes
EET 96029	2.5	7–9	nd	No
Murray	2.4–2.5	7–8	S1[e]	No

[a] After Rubin et al. (2007).
[b] Uses the 'without rim' aspect ratio values from Table 2, and assumes a *single* shock event. The pressure values have been obtained by comparing mean aspect ratios of sample chondrules with the correlations between chondrule aspect ratios and shock pressure obtained experimentally by Tomeoka et al. (1999) for Murchison (CM2) and Nakamura et al. (2000) for Allende (CV3) (Fig. 10). nd denotes not determined.
[c] From Rubin (2012).
[d] From Nakamura et al. (2000).
[e] From Scott et al. (1992).

have sought other indicators of hypervelocity impact in our samples, one of which is the presence of fractures. The experiments of Tomeoka et al. (1999) on Murchison showed that 1–2 μm sized randomly oriented fractures form in the matrix at 10 GPa. Fractures are greater in size and density in the higher pressure experiments, attaining ~50 μm width at 30 GPa. The fractures that form at these higher pressures are predominantly oriented normal or at a high angle to the compression axis. Melt was observed in those samples shocked to 28 GPa and higher (Tomeoka et al., 1999), and there is a catastrophic disruption at 30–35 GPa (Tomeoka et al., 2003).

Several samples used in the present study contain open fractures and/or veins of calcite, dolomite or gypsum. LON 94101 and QUE 93005 each have a single carbonate vein. The calcite vein in LON 94101 is oriented at a high angle to the petrofabric (Fig. 3c), and the dolomite vein in QUE 93005 lies parallel to the petrofabric (Fig. 3e). Both orientations (high-angle and parallel to the petrofabric) are consistent with an impact origin, although in LON 94101 and QUE 93005 these are only single veins. In SCO 06043 on the other hand, a network of dolomite veins lie sub-parallel to the petrofabric, and also fractures, partially filled with terrestrial gypsum, are oriented at a low angle to the dolomite veins (Fig. 3g). Although the gypsum is likely to be a product of terrestrial weathering, the dolomite veins are pre-terrestrial because they are cut by the fusion crust (Lindgren et al., 2012). Orientation of the dolomite veins and fractures both sub-parallel to the petrofabric suggests by analogy with the experiments by Tomeoka et al. (1999), that the tensional stresses sufficient to exceed the yield strength of the meteorite matrix were due to shock. Determinations of the tensile strength of CM carbonaceous chondrites have given values of ~0.3 to 30 MPa (Tsuchiyama et al., 2009), and 82 ± 6 MPa for Sutters Mill (Jenniskens et al., 2012). MET 01072 and LAP 031166 both have extensive networks of fractures; in LAP 031166 they are partially filled with gypsum (Figs. 3d, f and 2c, d). Their density and preferred orientation parallel and a high angle to the petrofabric is again strongly suggestive of fracturing in response to shock. Similar observations led Nakamura et al. (2012) to infer that MET 01072 had been shocked to 10 GPa. Further, Alexander et al. (2013) showed that MET 01072 has been heated, which would also be consistent with impact shock. We conclude that the following meteorites have been shocked to pressures sufficient to open fracture networks whose long axes are parallel and/or normal to the axis of compression (i.e., >~10 GPa): SCO 06043, MET 01072, LAP 031166. As fractures in SCO 06043 were cemented by carbonate, they must have formed prior to completion of aqueous alteration. The single veins in LON 94101 and QUE 93005 are still consistent with impact origin but with much lower intensity of fracturing.

4.6. The Murchison paradox

4.6.1. Variability of Murchison

Murchison had a relatively large recovered mass (~100 kg) and is described as a regolith breccia, so the degree of shock and deformation could vary throughout the meteorite. Scott et al. (1992) found that olivine grains displayed different levels of shock and therefore assigned Murchison to a shock stage ranging from S1 to S2. On the other hand, Tomeoka et al. (1999) and Rubin (2012) designated Murchison to shock stage S1. Previous studies have found different degrees of petrofabric development in Murchison. Rubin (2012) did not find a significant petrofabric (only 17% of particles within 10° of the median azimuth), and Tomeoka et al. (1999) recorded an average chondrule aspect ratio of only 1.17 ± 0.13 in the control sample that had not undergone experimental impacts. Fujimura et al. (1983) used X-ray pole figure goniometry and found a weak petrofabric defined by a preferred orientation of matrix phyllosilicate. Hanna et al. (2012), however, identified a reasonably strong petrofabric defined by XCT dark objects with an average aspect ratio of 1.53 ± 0.21, but which is significantly lower than the chondrule aspect ratio in the present study of 1.75 ± 0.39. Uesugi et al. (2013) used synchrotron radiation XCT to study carbonaceous chondrites including Murchison. Although they did not quantify petrofabrics, the elongate and aligned segmented objects they described in Murchison (Fig. A1.5; Uesugi et al., 2013) indicate that it is present. Barber (1981) described carbonate veins in Murchison, but their origin is unknown.

Rubin (2012) and Tomeoka et al. (1999) did not observe a petrofabric in Murchison, while the other studies have. This may be explained by the fact that while Rubin (2012) and Tomeoka et al. (1999) used 2D surfaces, the others were 3D studies; and as shown by the three faces of the Murchison block, the chondrule aspect ratio and petrofabric vary significantly depending on the orientation of the 2D surface relative to the petrofabric. However, although sample orientation relative to petrofabric is probably part of the explanation, it is likely that Murchison is heterogeneous with natural variations in the degree of shock between samples. This is reinforced by the finding that two samples of Murchison measured in 3D show markedly different aspect ratios (1.53 ± 0.21 (Hanna et al., 2012) *vs* 1.75 ± 0.39 (the present study)). Our sample is therefore from lithology with a stronger petrofabric.

4.6.2. Murchison: flattened chondrules but low shock stage

Most of the meteorites that contain high aspect ratio chondrules (i.e., LAP 031166, MET 01072, SCO 06043) have independent evidence of hypervelocity impact in the form of shock fractures or veins (Table 3). Therefore, we conclude that they have experienced at least one high intensity shock event. The pressures suggested for Murray, EET 96029, LON 94101 and QUE 93005 from their chondrule flattening (i.e., <10 GPa) are consistent with their S1 shock stages and the absence or scarcity of fractures/veins (both LON 94101 and QUE 93005 have a single carbonate vein, but neither form a fracture network). We therefore conclude that these four meteorites have undergone one or more episodes of low intensity shock. Note that the fine-scale contortion of the LON 94101 calcite vein shows that following the compression-extension event (to form the weak petrofabric and pre-calcite cementation fracture) the meteorite underwent compression along an axis normal to

the long axis of the vein, therefore demonstrating that this meteorite experienced at least two episodes of deformation (Lindgren et al., 2011). The anomaly here is Murchison, because it lacks the high density of fractures possessed by MET 01072 and LAP 031166, despite its chondrules having similar aspect ratios. Given the orientation of $\sigma_{1calcite}$ and $\sigma_{1chondrule}$ fractures should have developed normal to the +z side and +y side but none have been observed (Fig. 1). This suggests that our Murchison sample has not been shocked to pressures sufficient to generate fractures (i.e., probably <10 GPa), which would be consistent with the three previous determinations of its shock stage (Scott et al., 1992; Tomeoka et al., 1999; Rubin, 2012). Thus Murchison presents a paradox: How could a meteorite that has not been exposed to high shock pressures have a strong petrofabric defined by flattened chondrules?

One possible explanation that should at least be considered is that Murchison was highly shocked *prior* to aqueous alteration (at a CM3 stage), and the fractures that would have developed were healed by later extensive aqueous alteration. However, we suggest here that the explanation for this paradox is rather that our Murchison sample has experienced *multiple low intensity* impacts. There are several lines of evidence to support this conclusion. Firstly, the XCT data show that the chondrule short axes share a common orientation (i.e., are clustered in Fig. 7d), which represents $\sigma_{1chondrule}$. However, the orientations of the long axes are much less well constrained (Fig. 7c). Thus the chondrules are flattened in the same plane, which is at moderately high angle to the reference side of the block, but within this plane the chondrule long axes vary widely in their orientation. This pattern can therefore be interpreted to suggest that there were several shock waves, all propagating in roughly the same direction (i.e., $\sigma_{1chondrule}$). If the impacts took place while the sample was buried, the burial could have caused the overall flattening in one plane, which was then enhanced by several impacts with different orientations. Experimental impacts on Allende (CV3) by Nakamura et al. (2000) showed that the sample that was shocked twice had similar petrofabrics to the CV chondrites that have experienced the highest level of shock by natural impacts.

The second line of evidence for multiple events comes from the calcite *e*-twin stress analysis. σ_1 obtained from these data (i.e., $\sigma_{1calcite}$) lies at a high angle to the reference side, in common with $\sigma_{1chondrule}$, but is much more widely scattered. This we suggest reflects multiple mild shock impacts of at least ~0.1 to 0.5 GPa (the threshold shock pressure for twinning; Lindgren et al., 2013b), although some caution has to be employed in interpretation of the calcite twin stress analyses since individual calcite crystals could have been rotated after twin formation. However, multiple impacts are further confirmed by evidence from individual calcite crystals showing sets of cross-cutting *e*-twins (Fig. 6b). It is also possible that the calcite does not record the full impact record since some of the twin microstructures could have been healed if impact deformation occurred while fluids were still present.

The third line of evidence for multiple impacts comes from comparison of $\sigma_{1chondrule}$ and $\sigma_{1calcite}$. Whilst $\sigma_{1chondrule}$ is at a high angle to the reference side, $\sigma_{1calcite}$ is more widely spread. Crucially, however, the direction of $\sigma_{1chondrule}$ and $\sigma_{1calcite}$ differs measurably (Fig. 7a, d), which is interpreted as being due to multiple impact events. Calcite *e*-twins will record impacts during or after aqueous alteration, whereas chondrules may record earlier impacts that were of a higher magnitude (although still less than the threshold intensity required to open fractures). Evidence of differing stress orientations recorded in the same chondrite sample is rare, and is usually the result of different lithologies within an obvious breccia (Friedrich et al., 2013). Here, although Murchison is a microbreccia, only one lithology is present within the sample studied.

4.7. Shock and aqueous alteration

A general genetic link between parent body deformation and aqueous alteration of the CMs has been proposed in a number of previous studies (e.g., Richardson, 1981; Tomeoka and Buseck, 1985; Greenwood et al., 1994). The results of a quantitative analysis of petrofabrics in a suite of CMs led Rubin (2012) to develop a model that specifically links impact-induced deformation with alteration. The meteorite samples analysed for the present study show a weak anticorrelation between CM petrologic subtype and chondrule-defined petrofabric (Fig. 5b). Although the anticorrelation is relatively weak here ($r^2 = 0.35$), nevertheless it supports the suggestion by Rubin (2012) of a genetic relationship between the magnitude of alteration and intensity of impact compaction. However, in order for collisions to facilitate alteration, the impact(s) responsible for the petrofabrics must have taken place before and/or during aqueous activity. A first step in testing the model is therefore to explore the evidence for the relative chronology of deformation and alteration.

4.7.1. Timing of impacts relative to alteration

One interpretation of the correlation between collisions and alteration is that the petrofabric-forming impacts took place after aqueous processing and that the more highly altered meteorites deformed more readily on account of their greater proportion of ductile phyllosilicates. However, as illustrated in Fig. 10, for a given shock pressure chondrules in Murchison (partly hydrated) are flattened less than those in Allende (largely anhydrous), presumably due to attenuation of shock waves by the phyllosilicate-rich and porous CM matrix. Therefore if alteration predated impacts, high shock pressures and/or many lower intensity events would be required in order to achieve the level of chondrule flattening recorded by meteorites such as SCO 06043. Whilst this is not evidence against post-alteration shock, it could support the possibility. More importantly, a limit to the degree of flattening of chondrules caused by *single* impact shock in experimental work (e.g., Tomeoka et al., 1999), supports the high aspect ratios to be caused by *several* impacts.

Rubin (2012) described petrographic evidence from Nogoya (CM2.2) and MET 01070 (CM2.0) that impact fracturing predated alteration, and suggested that such a timing was typical for the CMs. He hypothesized that

Table 4
Descriptions of mineral veins in CM carbonaceous chondrites.

Meteorite	Vein mineralogy and petrography	Reference
Murchison (CM2.5)	Carbonates fill submicroscopic veins	Barber (1981)
LON 94101 (CM2.3)	Single mm-sized calcite vein	Lindgren et al. (2011)
Cold Bokkeveld (CM2.2)	Veins containing calcite, phyllosilicates, iron oxides and altered sulphides	Bunch and Chang (1980)
Cold Bokkeveld (CM2.2)	Carbonates fill submicroscopic veins	Barber (1981)
Cold Bokkeveld (CM2.2)	Polyphase gypsum veins	Lee (1993)
Cold Bokkeveld (CM2.2)	Numerous Ca-carbonate veins	Benedix et al. (2003)
Nogoya (CM2.2)	Veins containing calcite, phyllosilicates, iron oxides, altered sulphides	Bunch and Chang (1980)
Nogoya (CM2.2)	One Ca-carbonate vein	Benedix et al. (2003)
QUE 93005 (CM2.1)	Calcite and dolomite veins in the matrix and chondrule rims	Lee et al. (2012)
Sutter's Mill (CM2.1–2.0)	Veins of dolomite in chondrule rims	Jenniskens et al. (2012)
ALH 84051 (CM2.0)	Veins of granular dolomite	Tyra et al. (2009)
SCO 06043 (CM2.0)	Veins of dolomite	Lindgren et al. (2011)

collisions enhanced alteration because fractures formed by the impacts served as conduits or reservoirs for aqueous fluids; these solutions would have either initiated alteration or enhanced on-going reactions. Table 3 shows that the five most heavily compacted CMs in the present study (excluding Murchison) all have fractures or veins whose orientations relative to petrofabrics are consistent with an impact origin. The carbonate veins in LON 94101, QUE 93005 and SCO 06043 show that fracturing of these meteorites took place whilst aqueous solutions were present and so could potentially have facilitated alteration. The other two meteorites, LAP 0311660 and MET 01072, have a strong petrofabric together with abundant fractures, but there is no evidence for these fractures having contained pre-terrestrial water (the gypsum veins in LAP 031166 probably formed by Antarctic weathering). Therefore it cannot be stated with certainty that there is a genetic link between impact fracturing and alteration in these two CMs. Overall, however, there is good evidence to link vein formation to aqueous alteration of the host rock. Bunch and Chang (1980) were among the first to connect these two processes, and veins of likely pre-terrestrial carbonates have now been described in eight CMs, most of which are moderately or highly aqueously processed (Table 4). Alexander et al. (2013) also speculated that fracture distribution may account for heterogeneities in the degree of aqueous alteration between samples of the same CM meteorite. The presence of fractures in CM carbonaceous chondrite parent bodies is very likely given that C-type asteroids have porosities of 40–70% (Baer et al., 2011).

Murchison is the only meteorite in our sample set that has a strong chondrule-defined petrofabric but lacks fractures/veins; it is also the least altered CM studied. As discussed above, our Murchison sample probably underwent multiple low intensity impacts, none of which were sufficiently energetic to exceed the yield strength of the matrix and produce fractures. The presence of *e*-twins in the Murchison calcite grains shows that at least some of these impacts postdated carbonate precipitation. Therefore Murchison illustrates the general conclusion that despite the weight of evidence that the CMs have undergone impacts, these events would have facilitated alteration only if they were sufficiently energetic to open fractures, and then only if a reservoir of aqueous fluids was available and that could gain access to the fracture network.

4.7.2. Role of fracturing in facilitating alteration

For fractures to initiate or enhance alteration of a given CM, they would need to 'tap' a source of water that was previously unavailable to the parent body region from where the meteorite was derived. Evidence for the provenance of vein-filling minerals was provided by Lee et al. (2013) in an isotopic study of the LON 94101. They showed that the oxygen isotope composition of vein calcite is substantially different to that of grains of earlier formed aragonite and calcite within the enclosing meteorite matrix. Lee et al. (2013) concluded that the solutions from which the vein calcite precipitated were derived from a different parent body region that was substantially hotter or contained water that had undergone more reaction with original anhydrous silicates. Therefore in the case of LON 94101 at least, the pulse of new fluids would have enhanced alteration, rather than initiated it, as fracturing postdated precipitation of aragonite and calcite in the meteorite matrix. Results from the present study therefore find that some CMs underwent impacts of sufficient intensity to open fractures and at a time when aqueous solutions were still present, whereas others were fractured after alteration, and some were never exposed to stresses sufficient to exceed the yield strength of the matrix. These findings are unsurprising given the stochastic nature of impacts, and the likely spatial and temporal variability of parent body internal structure.

5. CONCLUSIONS

In the introduction we highlighted a striking paradox within the CM carbonaceous chondrites: almost all have a S1 shock stage, but many have also undergone sufficient compaction to develop foliation petrofabrics. Three origins for these petrofabrics were proposed: (i) lithostatic compaction; (ii) attenuation of energy from a single high-energy impact; (iii) multiple low energy shock events. Of the eight CMs studied, six have a petrofabric defined by flattened chondrules, which we propose formed in response to impacts rather than overburden pressure. Independent evidence for impacts comes from the presence of fractures and

veins in five of the CMs. Empirical relationships between shock pressure and chondrule aspect ratio that were obtained by Tomeoka et al. (1999) and Nakamura et al. (2000) suggest that the degree of flattening observed in chondrules from LAP 031166, MET 01072, Murchison and SCO 06043 would require a single shock event of $>\sim$18 GPa. Given that MET 01072 has been heated, this CM may indeed have experienced such pressures, but the other three are very unlikely to have been so highly shocked. We therefore conclude that chondrule-defined petrofabrics in most CMs have formed in response to multiple low energy impacts.

The role of multiple impacts in deformation of the CMs is underscored by Murchison. This meteorite has a strong petrofabric indicating in-situ deformation, but is devoid of fractures and veins. Twins in calcite grains show that the sample we studied has experienced multiple $>\sim$0.1 to 0.5 GPa shock events, and further evidence for repeated impacts has come from analysis of petrofabrics in 3D by X-ray computed tomography. Multiple impacts are evident from (i) the chondrules are flattened in the same plane, but oriented with multiple directions within this plane, (ii) calcite twin stress analyses show scattering of σ_1 in several orientations and calcite grains show multiple phases of calcite twinning, (iii) the stress that caused the chondrule petrofabric had a different direction from the stress that caused the calcite twinning, i.e., $\sigma_{1\text{chondrule}} \neq \sigma_{1\text{calcite}}$. Comparison between XCT of the Murchison block and SEM imaging of the three faces of the Murchison block shows that reliable results can be obtained from XCT analyses, with the caveat that mineralogically different types of chondrules cannot be distinguished in the XCT volume.

Our results support the hypothesis of Rubin (2012) that shock fracturing of the CMs has facilitated their aqueous processing. The presence of carbonate veins in LON 94101, QUE 93005 and SCO 06043 is clear evidence for impact fracturing before or during alteration. Results from previous oxygen isotope analysis of the LON 94101 vein show that it precipitated from aqueous solutions from another parent body region that exploited the fracture. LAP 031166 and MET 01072 both contain fracture networks but lack pre-terrestrial mineral veins and so either the impact(s) that led to brittle deformation took place after alteration, or solutions that were once present within the fractures did not precipitate any secondary minerals.

This study further highlights the spatial and temporal complexity of CM carbonaceous chondrite parent body environments. Taken together with Rubin (2012), our results have provided the evidence that impacts were a significant determinant of the physical, chemical, isotopic, mineralogical, and probably also the thermal evolution of CM chondrites. We do not suggest that aqueous solutions accessed the parent body regions from where the CMs were derived solely by fracture-mediated fluid flow. Rather we propose that in some cases brittle deformation accompanying impacts facilitated fluid movement, probably on metre-plus length scales, and these solutions are likely to have facilitated aqueous alteration of the matrix and chondrules.

ACKNOWLEDGEMENTS

We thank the three reviewers for thorough comments that substantially improved this manuscript. We acknowledge Peter Chung, John Gilleece, William Smith and Colin How at the University of Glasgow and Tristan Lowe at the Manchester X-ray imaging facility for technical support. Thanks to Jordan Wright, University of Glasgow, for help with chondrule measurements in the SEM. Thanks to Richard Ketcham, University of Texas, for helpful comments on the manuscript. Thanks to Jon Friedrich, Fordham University, for helpful discussions regarding the statistical analysis of orientation data and for help with the Stereo32 software. Thanks to Daniel Koehn at the University of Glasgow for helping with stereonets. We are grateful to the UK Science and Technology Facilities Council – Grants ST/G001693/1 and ST/K000942/1 for funding this work. K.J.D. wishes to acknowledge UK Engineering and Physical Sciences Research Council – Grant EP/I02249X/1, which supports the Manchester X-ray Imaging Facility, and the Research Complex at Harwell. R.D.H. is supported by the NASA Earth and Space Sciences Fellowship Program – Grant NNX13AO64H. We are grateful to the NASA meteorite collection and Caroline Smith at NHM for loan of samples.

REFERENCES

Alexander C. M. O', Howard K. T., Bowden R. and Fogel M. L. (2013) The classification of CM and CR chondrites using bulk H, C and N abundances and isotopic compositions. *Geochim. Cosmochim. Acta* **123**, 244–260.

Baer J., Chesley S. R. and Matson R. D. (2011) Astrometric masses of 26 asteroids and observations on asteroid porosity. *Astron. J.* **141**(143), 1–12.

Barber D. J. (1981) Matrix phyllosilicates and associated minerals in C2M carbonaceous chondrites. *Geochim. Cosmochim. Acta* **45**, 945–970.

Barber D. J. and Wenk H.-R. (1979) Deformation twinning in calcite, dolomite, and other rhombohedral carbonates. *Phys. Chem. Miner.* **5**, 141–165.

Benedix G. K., Leshin L. A., Farquhar J., Jackson T. and Thiemens M. H. (2003) Carbonates in CM2 chondrites: constraints on alteration conditions from oxygen isotopic compositions and petrographic observations. *Geochim. Cosmochim. Acta* **67**, 1577–1588.

Brearley A. J. and Papike J. J. (1993) Carbonaceous chondrite clasts in the Kapoeta Howardite. *Lunar Planet. Sci XXIV*. Lunar Planet. Inst., Houston. Part 1, A–F, pp. 183–184 (abstr.).

Bunch T. E. and Chang S. (1980) Carbonaceous chondrites-II. Carbonaceous chondrite phyllosilicates and light element geochemistry as indicators of parent body processes and surface conditions. *Geochim. Cosmochim. Acta* **44**, 1543–1577.

Burkhard M. (1993) Calcite twins, their geometry, appearance and significance as stress–strain markers and indicators of tectonic regime: a review. *J. Struct. Geol.* **15**, 351–368.

Cain P. M., McSween H. Y. and Woodward N. B. (1986) Structural deformation of the Leonville chondrite. *Earth Planet. Sci. Lett.* **77**, 165–175.

De Bresser J. H. P. and Spiers C. J. (1997) Strength characteristics of the r, f, and c slip systems in calcite. *Tectonophysics* **272**, 1–23.

de Leuw S., Rubin A. E. and Wasson J. T. (2010) Carbonates in CM chondrites: Complex formational histories and comparison to carbonates in CI chondrites. *Meteorit. Planet. Sci.* **45**, 513–530.

Dodd R. T. (1965) Preferred orientation of chondrules in chondrites. *Icarus* **4**, 308–316.

Ebel D. S. and Rivers M. L. (2007) Meteorite 3-D synchrotron microtomography: methods and applications. *Meteorit. Planet. Sci.* **42**, 1627–1646.

Friedrich J. M., Weisberg M. K. and Rivers M. L. (2013) A record of the sequence and intensity of multiple impacts in the NWA 7298 H chondrite. *Met. Soc. Meeting LXXVI*, Edmonton. #5236 (abstr.).

Fuchs L. H., Olsen E. and Jensen K. J. (1973) Mineralogy, mineralchemistry, and composition of the Murchison (C2) meteorite. *Smithson. Contrib. Earth Sci.* **10**, 39.

Fujimura A., Kato M. and Kumazawa M. (1982) Preferred orientation of phyllosilicates in Yamato-74642 and -74662, in relation to deformation of C2 chondrites. *Proc. NIPR Symp. Ant. Met.* **7**, 207–215.

Fujimura A., Kato M. and Kumazawa M. (1983) Preferred orientation of phyllosilicate [001] in matrix of Murchison meteorite and possible mechanisms of generating the oriented texture in chondrites. *Earth Planet. Sci. Lett.* **66**, 25–32.

Gattacceca J., Rochette P., Denise M., Consolmagno G. and Falco L. (2005) An impact origin for the foliation of chondrites. *Earth Planet. Sci. Lett.* **234**, 351–368.

González-Casado J. M. and García-Cuevas C. (1999) Calcite twins from microveins as indicators of deformation history. *J. Struct. Geol.* **21**, 875–889.

González-Casado J. M., Gumiel P., Giner-Robles J. L., Campos R. and Moreno A. (2006) Calcite e-twins as markers of recent tectonics: insights from Quaternary karstic deposits from SE Spain. *J. Struct. Geol.* **28**, 1084–1092.

Graham D. J. and Midgley N. G. (2000) Graphical representation of particle shape using triangular diagrams; an Excel spreadsheet method. *Earth Surf. Proc. Land.* **25**, 1473–1477.

Greenwood R. C., Lee M. R., Hutchison R. and Barber D. J. (1994) Formation and alteration of CAIs in Cold Bokkeveld (CM2). *Geochim. Cosmochim. Acta* **58**, 1913–1935.

Hanna R. D., Ketcham R. A. and Hamilton V. E. (2012) Inclusion foliation in Murchison as revealed by high resolution X-ray CT. *Lunar Planet. Sci. XLIII*. Lunar Planet. Inst., Houston. #1242 (abstr.).

Jenniskens P., Fries M. D., Qing-Zhu Y., Zolensky M. E., Krot A. N., Sanford S. A., Sears D., Bauford R., Ebel D. S., Friedrich J. M., Nagashima K., Wimpenny J., Yamakawa A., Nishiizumi K., Hamajima Y., Caffee M., Weten K. C., Laubenstein M., Davis A., Simon S. B., Heck P. R., Young E. D., Kohl I. E., Thimens M. H., Nunn M. H., Mikouchi T., Hagiya K., Ohsumi K., Cahill T. A., Lawton J. A., Barnes D., Steele A., Rochette P., Verosub K. L., Gattacceca J., Cooper G., Glavin D. P., Burton A. S., Dworkin J. P., Elsila J. E., Pizzarello S., Ogliore R., Schitt-Kopplin P., Harir M., Hertkorn N., Verchovsky S., Grady M., Nagao K., Okazaki R., Takechi H., Hirori T., Smith K., Silber E. A., Brown P. G., Albers J., Klotz D., Hankey M., Matson R., Fries J. A., Walker R. J., Puchtel I., Lee C.-T. A., Erdman M. E., Eppich G. R., Roeske S., Gabelica Z., Lerche M., Nuevo M., Girten B. and Worden S. P. (2012) Radar-enabled recovery of the Sutter's Mill meteorite, a carbonaceous chondrite regolith breccia. *Science* **338**, 1583–1587.

Ketcham R. A. (2005a) Computational methods for quantitative analysis of three-dimensional features in geological specimens. *Geosphere* **1**, 32–41.

Ketcham R. A. (2005b) Three-dimensional grain fabric measurements using high-resolution X-ray computed tomography. *J. Struct. Geol.* **27**, 1217–1228.

Ketcham R. A. and Carlson W. D. (2001) Acquisition, optimization, and interpretation of X-ray computed tomographic imagery: applications to the geosciences. *Comput. Geosci.* **27**, 383–400.

Kerridge J. F. and Bunch T. E. (1979) Aqueous activity on asteroids: evidence from carbonaceous chondrites. In *Asteroids* (ed. T. Gehrels). Univ. Arizona Press, Tucson, Arizona, pp. 745–764.

Lee M. R. (1993) The petrography, mineralogy and origins of calcium sulphate within the Cold Bokkeveld CM carbonaceous chondrite. *Meteoritics* **28**, 53–62.

Lee M. R., Bland P. A. and Graham G. (2003) Preparation of TEM samples by focused ion beam (FIB) techniques: applications to the study of clays and phyllosilicates in meteorites. *Mineral. Mag.* **67**, 581–592.

Lee M. R. and Ellen R. (2008) Aragonite in the Murray (CM2) carbonaceous chondrite: implications for parent body compaction and aqueous alteration. *Meteorit. Planet. Sci.* **43**, 1219–1231.

Lee M. R., Lindgren P., Sofe M. R., Alexander C. M. O'D. and Wang J. (2012) Extended chronologies of aqueous alteration in the CM2 carbonaceous chondrites: evidence from carbonates in Queen Alexandra Range 93005. *Geochim. Cosmochim. Acta* **92**, 148–169.

Lee M. R., Sofe M. R., Lindgren P., Starkey N. A. and Franchi I. A. (2013) The oxygen isotope evolution of parent body aqueous solutions as recorded by multiple carbonate generations in the Lonewolf Nunataks 94101 CM2 carbonaceous chondrite. *Geochim. Cosmochim. Acta* **121**, 452–466.

Lee M. R., Lindgren P. and Sofe M. R. (2014) Aragonite, breunnerite, calcite and dolomite in the CM carbonaceous chondrites: high fidelity recorders of progressive parent body aqueous alteration. *Geochim. Cosmochim. Acta* **144**, 126–156.

Lindgren P. and Lee M. R. (2014) Glassy chondrule mesostasis in EET 96029: a CM3 component of a minimally altered CM2 carbonaceous chondrite. *77th Meteoritical Society Meeting*. #5276 (abstr.).

Lindgren P., Lee M. R., Sofe M. and Burchell M. J. (2011) Microstructure of calcite in the CM2 carbonaceous chondrite LON 94101: implications for deformation history during and/or after aqueous alteration. *Earth Planet. Sci. Lett.* **306**, 289–298.

Lindgren P., Lee M. R. and Sofe M. (2012) Evidence for multiple fluid pulses in the CM1 carbonaceous chondrite parent body. *Lunar Planet. Sci. XLIII*. Lunar Planet. Inst., Houston. #1949 (abstr.).

Lindgren P., Lee M. R., Sofe M. R. and Zolensky M. E. (2013a) Clasts in the CM2 carbonaceous chondrite Lonewolf Nunataks 94101: evidence for aqueous alteration prior to complex mixing. *Meteorit. Planet. Sci.* **48**, 1074–1090.

Lindgren P., Price M. C., Lee M. R. and Burchell M. J. (2013b) Constraining the pressure threshold of impact induced calcite twinning: implications for the deformation history of aqueously altered carbonaceous chondrites. *Earth Planet. Sci. Lett.* **384**, 71–80.

Metzler K., Bischoff A. and Stöffler D. (1992) Accretionary dust mantles in CM chondrites: evidence for solar nebula processes. *Geochim. Cosmochim. Acta* **56**, 2873–2897.

Martin P. M., Mills A. A. and Walker E. (1975) Preferential orientation in four C3 chondritic meteorites. *Nature* **252**, 37–38.

Martin P. M. and Mills A. A. (1980) Preferred orientations in meteorites. *Earth Planet. Sci. Lett.* **51**, 18–25.

Nakamura T. (2006) Yamato 793321 CM chondrite: dehydrated regolith material of a hydrous asteroid. *Earth Planet. Sci. Lett.* **242**, 26–38.

Nakamura T., Tomeoka K., Sekine T. and Takeda H. (1995) Impact-induced chondrule flattening in the Allende CV3 carbonaceous chondrite: shock experiments. *Meteoritics* **30**, 344–347.

Nakamura T., Tomeoka K., Takaoka N., Sekine T. and Takeda H. (2000) Impact-induced textural changes of CV carbonaceous chondrites: experimental reproduction. *Icarus* **146**, 289–300.

Nakamura T., Yoshioka K., Nakato A. and Miyahara M. (2012) First discovery of a heavily shocked CM carbonaceous chondrite. *Japan Geoscience Union Meeting*. PPS05-09 (abstr.).

Nelson V. E. and Rubin A. E. (2002) Size-frequency distributions of chondrules and chondrule fragments in LL3 chondrites: implications for parent-body fragmentation of chondrules. *Meteorit. Planet. Sci.* **37**, 1361–1376.

Olsen E. J., Davis A. M., Hutcheon I. D., Clayton R. N., Mayeda T. K. and Grossman L. (1988) Murchison xenoliths. *Geochim. Cosmochim. Acta* **52**, 1615–1626.

Reid A. M., Buchanan P., Zolensky M. E. and Barrett R. A. (1990) The Bholghati howardite: petrography and mineral chemistry. *Geochim. Cosmochim. Acta* **54**, 2161–2166.

Richardson S. M. (1981) Alteration of mesostasis in chondrules and aggregates from three C2 carbonaceous chondrites. *Earth Planet. Sci. Lett.* **52**, 67–75.

Roth A. S. G., Baur H., Heber V. S., Reusser E. and Wieler R. (2011) Cosmogenic helium and neon in individual chondrules from Allende and Murchison: implications for the precompaction exposure history of chondrules. *Meteorit. Planet. Sci.* **46**, 989–1006.

Rubin A. E. (2012) Collisional facilitation of aqueous alteration of CM and CV carbonaceous chondrites. *Geochim. Cosmochim. Acta* **90**, 181–194.

Rubin A. E. and Swindle T. D. (2011) Flattened chondrules in the LAP 04581 LL5 chondrite: evidence for an oblique impact into LL3 material and subsequent collisional heating. *Meteorit. Planet. Sci.* **46**, 587–600.

Rubin A. E., Trigo-Rodríges J. M., Huber H. and Wasson J. T. (2007) Progressive aqueous alteration of CM carbonaceous chondrites. *Geochim. Cosmochim. Acta* **71**, 2361–2382.

Scott E. R. D., Keil K. and Stöffler D. (1992) Shock metamorphism of carbonaceous chondrites. *Geochim. Cosmochim. Acta* **56**, 4281–4293.

Schedl A. (2006) Application of twin analysis to studying meteorite impact structures. *Earth Planet. Sci. Lett.* **244**, 530–540.

Sneed E. D. and Folk R. L. (1958) Pebbles in the lower Colorado River, Texas; a study in particle morphogenesis. *J. Geol.* **66**, 114–150.

Sneyd D. S., McSween H. Y., Sugiura N., Strangway D. W. and Nord, Jr., G. L. (1988) Origin of petrofabric and magnetic anisotropy in ordinary chondrites. *Meteoritics* **23**, 139–149.

Spang J. H. (1972) Numerical method for dynamic analysis of calcite twin lamellae. *Geol. Soc. Am. Bull.* **83**, 467–472.

Stöffler D., Keil K. and Scott E. R. D. (1991) Shock metamorphism of ordinary chondrites. *Geochim. Cosmochim. Acta* **55**, 3845–3867.

Tomeoka K. and Buseck P. R. (1985) Indicators of aqueous alteration in CM carbonaceous chondrites: microtextures of a layered mineral containing Fe, S, O, and Ni. *Geochim. Cosmochim. Acta* **49**, 2149–2163.

Tomeoka K., Yamahana Y. and Sekine T. (1999) Experimental shock metamorphism of the Murchison CM carbonaceous chondrite. *Geochim. Cosmochim. Acta* **21**, 3683–3703.

Tomeoka K., Kiriyama K., Nakamura K., Yamahana Y. and Sekine T. (2003) Interplanetary dust from the explosive dispersal of hydrated asteroids by impacts. *Nature* **423**, 60–62.

Tourneret C. and Laurent P. (1990) Paleo-stress orientations from calcite twins in the North Pyrenean foreland, determined by the Etchecopar inverse method. *Tectonophysics* **180**, 287–302.

Trigo-Rodriguez J. M., Rubin A. E. and Wasson J. T. (2006) Non-nebular origin of dark mantles around chondrules and inclusions in CM chondrites. *Geochim. Cosmochim. Acta* **70**, 1271–1290.

Tsuchiyama A., Mashio E., Imai Y., Noguchi T., Miura Y., Yano H. and Nakamura T. (2009) Strength measurement of carbonaceous chondrites and micrometeorites using compression testing machine. *Met. Soc. Meeting LXXII*, Nancy. #5189 (abstr.).

Turner F. J. (1953) Nature and dynamic interpretation of deformation lamellae in calcite of three marbles. *Am. J. Sci.* **251**, 276–298.

Turner F. J. (1962) "Compression" and "tension" axes determined from {01–12} twinning in calcite. *J. Geophys. Res.* **67**, 1660.

Turner F. J. and Weiss L. E. (1963). In *Structural Analysis of Metamorphic Tectonites* (ed. R. R. Shrock). McGraw-Hill Book Company, Inc., New York, p. 545.

Tyra M. A., Brearley A. J., Hutcheon I. D., Ramon E., Matzel J. and Weber P. (2009) Carbonate formation timescales vary between CM1 chondrites ALH 84051 and ALH 84034. *Lunar Planet. Sci. XL*. Lunar Planet. Inst., Houston. #2474 (abstr.).

Uesugi M., Uesugi K., Takeuchi A., Suzuki Y., Hoshino M. and Tsuchiyama A. (2013) Three-dimensional observation of carbonaceous chondrites by synchrotron radiation X-ray CT – quantitative analysis and developments for the future sample return missions. *Geochim. Cosmochim. Acta* **116**, 17–32.

Velbel M. A., Tonui E. K. and Zolensky M. E. (2013) Compositions of partially altered olivine and replacement serpentine in the CM2 chondrite QUE 93005. *Met. Soc. Meeting LXXVI*, Edmonton. #5321 (abstr.).

Woodcock N. H. (1977) Specification of fabric shapes using an eigenvalue method. *Geol. Soc. Am. Bull.* **88**, 1231–1236.

Woodcock N. H. and Naylor M. A. (1983) Randomness testing in three-dimensional orientation data. *J. Struct. Geol.* **5**, 539–548.

Zolensky M. E. and Ivanov A. (2003) The Kaidun microbreccia meteorite: a harvest from the inner and outer asteroid belt. *Chem. Erde* **63**, 185–246.

Zolensky M. E., Barrett R. A. and Ivanov A. V. (1991) Mineralogy and matrix composition of clasts in the chondritic breccias Kaidun. *Lunar Planet. Sci. XXII*. Lunar Plant. Inst., Houston. #1565 (abstr.).

Zolensky M. E., Mittlefehldt D. W., Lipschutz M. E., Wang M.-S., Clayton R. N., Mayeda T. K., Grady M. M., Pillinger C. and Barber D. (1997) CM chondrites exhibit the complete petrologic range from type 2 to 1. *Geochim. Cosmochim. Acta* **61**, 5099–5115.

Associate editor: Chris Herd